Ray Analysis of Tapered Graded-Index Planar Waveguides and Fibers

by

Voravut Suppanitchakij

Thesis submitted to the Faculty of the
Virginia Polytechnic Institute and State University
in partial fulfillment of the requirements for the degree of
Master of Science
in
Electrical Engineering

APPROVED:

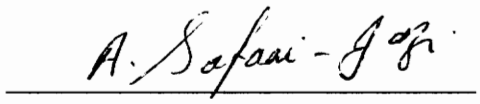

Ahmad Safaai-Jazi, Chairman

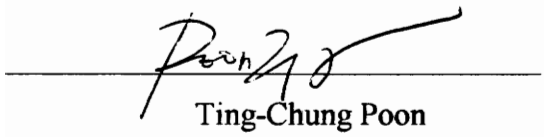

Ting-Chung Poon

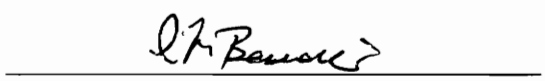

Ioannis M. Besieris

August 1995

Blacksburg, Virginia

Key words: Tapered waveguide, Ray trajectories, Graded-Index

Ray Analysis of Tapered Graded-Index Planar Waveguides and Fibers

by

Voravut Suppanitchakij

Ahmad Safaai-Jazi, Chairman

Electrical Engineering

(ABSTRACT)

Propagation properties of linearly tapered parabolic-index optical waveguides are investigated. Tapers with planar (two-dimensional) and fiber (three-dimensional) geometries are considered. A ray optics approach is used in the analysis, assuming that the characteristic dimensions of tapered waveguides are small compared to the wavelength of light.

Closed form analytical solutions are obtained for ray trajectories in tapers with small slope and small index difference between the core and cladding. To assess the accuracy of analytical solutions, exact ray trajectories in planar waveguides are determined using numerical techniques and compared to those obtained from the analytical method. The agreement between the analytical and numerical solutions is excellent.

It is observed that ray trajectories exhibit the behavior of modulated sinusoidal functions with decreasing amplitude and period as light travels toward the smaller end of the taper. This illustrates the power concentrating capability of the taper.

Applications of these graded-index tapers when used to couple power from light sources to planar and fiber waveguides and when they are used to connect two waveguides of different core sizes are addressed. Coupling efficiencies for light source coupling and radiation loss of tapers when used to connect two dissimilar waveguides are calculated. Numerical results for example cases are provided. A novel application of the taper as collimated beam concentrator is also proposed.

Abstract

Acknowledgments

I would like to express my sincere gratitude to Dr. Ahmad Safaai-Jazi for serving as my advisor and providing me with a very interesting topic for my thesis. Without his guidance and patience, the undertaking and completion of this thesis would not have been possible. He was always willing to share his valuable time to teach me how to conduct this study and always there to help me through these rough years. It has been my great pleasure to have been taught by such great man. There are no words to express the extent of my appreciation for all knowledge and expertise he has contributed. My respect for him continues to grow and I will be forever grateful. I would also like to thank the members of my committee, Dr. Ting-Chung Poon and Dr. Ioannis M. Besieris, for their helpful comments and suggestions.

I would especially like to extend my deep gratitude and appreciation to my parents, sisters and brother for all their love and support.

I finally wish to express my thanks to the person who has been very special to me during the writing of this thesis, Miss Kanokporn Kunchaicharoenkul. Thanks Nim, for being so loving and supportive.

Table of Contents

List of Figures

1. Introduction

Efficient launching of optical power from a source into a waveguide or fiber is of important consideration in optical communication systems. At a first glance, butt coupling of light sources to fibers appears to be simple and efficient; however, it usually results in poor coupling efficiency due to the different mode profiles of the source and fiber. Low-loss chip-to-fiber butt coupling can be achieved by means of on-chip spot-size transformers [1]. Two simple versions using laterally tapered InP-InGaAsP waveguides at the 1.55 μm wavelength have been fabricated. One consists of two differently tapered layers, while the other includes only one taper. The optimum insertion loss for a single transformer without antireflection coating, including Fresnel losses, amounts to about 1.1 dB. By using a fiber-coupling tapered semiconductor waveguide, a highly efficient spot-size converter (SSC) has been obtained [2]. The waveguide core of this device consists of InGaAsP for semiconductor chip coupling and an InP/InAlAs multiple quantum well (MQW) for single-mode fiber (SMF) coupling. To expand the chip spot size to that of SMF's, the equivalent refractive index of the MQW core is

adjusted by controlling the well-to-barrier-layer thickness ratio. A high coupling efficiency of 1.4 dB was obtained and the lateral and axial misalignment tolerances for SSC were 3 times better than those for conventional semiconductor waveguides.

The lateral focusing characteristics of planar microlens fabricated by the electromigration method has been studied in [3]. Its lateral focusing spot of 3 μm x 7 μm diameter is comparable with the mode size of single-mode fibers and planar microlenses relay optics can be constructed using this kind of lenses. It has been noted that planar microlens produced by the electromigration method has a desirable index distribution that resembles that of a Luneburg lens. By stacking two planar microlenses, a nearly circular focused spot of ~ 5-μm diameter, which is comparable to the mode-field-diameter of a single-mode fibers, has been obtained by lateral focusing [4].

Tapered waveguides and fibers have also been used frequently in the past in order to improve coupling of light sources to fibers [5]-[9]. In 1979, Uematsu and Ozeki have studied the power coupling between a multiheterojunction LED and a taper-ended multimode fiber, and achieved more than 50 % coupling efficiency. By using a tapered hemispherical-end fiber, which is obtained by heating and drawing the fiber between two arc electrodes, a coupling efficiency of 83 percent was achieved between a semiconductor laser and a nylon coated graded index multimode fiber [6]. In 1980, this technique was extended to single-mode fibers and resulted in a coupling efficiency of more than 35 percent [7]. Later, the coupling efficiency between monomode fibers and laser diodes was improved to more than 50 percent by means of a high index microlens

which is attached to the cleaved end of a tapered monomode fibre [8]. In 1989, another device for coupling single-mode fibers to laser diodes, consisting of a spherical ruby lens and a single-mode optical fiber up-taper, was introduced [9]. With this method, more than 60 percent of the light form the lens is coupled into a single-mode fiber via the taper. Tapered fibers have also found other important applications, including optical directional coupler [10], mode filter, and mode analyzer [11], vibration sensor [12], gas detection [13], and fluorescent sensors [14].

Grating couplers have also been studied [15]. They couple the light by diffracting an incident beam off a grating on the surface of the waveguide either into or out of the planar waveguide (depending on whether the grating is used as an input or an output coupler). Since the coupler is incorporated into the waveguide structure, then alignment problems are eliminated.The grating coupler can be designed to obtain relatively high coupling efficiencies; a theoretical maximum of 81% for an incident Gaussian beam has been reported in [16]. The combination of a tapered film and a grating coupler has also been studied [17]. A hybrid coupler with an increased acceptance angle, because of the taper, and high coupling efficiency and easier input beam positioning, because of characteristics of the grating coupler, can then be obtained. Waveguide grating couplers that have surface corrugation on both boundaries of the waveguide have been investigated too [18]. The presence of the double-surface corrugation produces dramatic results for the maximum measured coupling branching ratio (98%) and input coupling efficiency (78%).

The beginning of the graded-index optics can be traced back to about 1936 when R.K. Luneberg studied the properties of a peculiar type of lens, which has since come to be known as Luneberg lens. This lens has the ability to form an image from any direction with no distortion. The property of focusing energy in any direction with no distortion made the Luneberg lens very popular for a number of radar applications. The next major contribution was the development of vacuum furnace techniques for producing ultrapure silicon crystals for production of the transistors and for the controlled doping of slices of silicon crystals. These techniques eventually made possible the production of graded index fibers. If a glass rod is placed in a vacuum furnace and a gaseous dopant is introduced into the furnace, the dopant will penetrate into the glass rod that is held in the plastic state. Once doped, the rod can be drawn out in a fiber-drawing operation similar to the one used with the step-index preform. There is an alternative procedure. If the original glass billet is a tube instead of a rod, the diffusion process can proceed from the inside out with the dopant being a material that increases the index of refraction. In this case, after the doping process is complete, the tube is heated further and collapsed before drawing into fibers. In either case, the result is a material which has the highest index along the axis and the lowest index around the outside. In some respects this is a step-index fiber with an infinite number of steps.

Propagation of light in graded-index media has been studied before [19]-[22]. Beam propagation in gradient refractive-index media has been studied by using ABCD matrices to treat optical systems [19]. Numerical ray tracing has been developed to

determine ray trajectories in inhomogeneous media [20]. For planar waveguides with linearly graded-index profiles, exact analytical solutions for TE modes have been obtained [21]. Geometrical optics analysis of graded-index cylindrical fibers has also been presented [22].

Graded-index tapers have been studied by various researches, [23]-[27]. A study of focal curves generated by one-dimensional (1-D) gradient-index (GRIN) tapers with plane symmetry is given in [23]. The proposed method is based on illuminating, in a transverse direction, the 1-D GRIN taper to give rise to two-dimensional (or three-dimensional) focal curves. Focusing capabilities of a nonplanar symmetric GRIN profile was later extended [24]. In [25], tapered dielectric waveguides have been studied as light concentrators for illumination and solar energy applications. Their capability to collect and transmit high fluxes of light energy were investigated both theoretically and experimentally. Furthermore, GRIN rods are considered as matching devices, to improve the collecting performance of tapered guides. Beam propagation in tapered quadratic-index waveguides has been discussed in [26]. Several taper functions were investigated and several exact analytical solutions, presented in the standard ABCD beam matrix form, were derived for the propagation of off-axis polynomial-Gaussian beams. Approximate solutions that can be applied to more general types of tapers by the WKB method have also been obtained. Beam propagation in a special case of parabolically tapered graded-index waveguides has been studied and analytical solutions for the propagating fields and ray trajectories have been obtained [27].

Among various types of graded-index tapers, those with parabolic-index profile are of particular interest, because they can be fabricated, at low costs, using the available parabolic-index fibers or preforms. Much of the analysis of tapered waveguides and fibers in the literature are limited to step-index profiles or single-mode propagation. It appears that a comprehensive ray analysis of parabolic-index planar waveguides and fibers has not been presented so far. Such ray analysis is undertaken here.

In this thesis, propagation properties of linearly tapered multimode parabolic-index waveguides and fibers are investigated using a geometrical optics approach. First, Maxwell's equation are used to derive the ray equation in a general graded-index medium by assuming that characteristic dimensions of the medium are many times larger than the wavelength of the electromagnetic signal. The ray equation, derived in Chapter 2, forms the foundation of the geometrical optics analysis of parabolic-index tapers. Since the transverse dimensions of the tapers are assumed to be large compared with the wavelength of light, the ray optics approach is sufficiently accurate and provides a simple description of the light concentration capability of such tapers. Two-dimensional linearly tapered parabolic-index planar waveguides are examined in Chapter 3. An analytical solution of ray equation is obtained for tapers with small angles and small index difference between the core and cladding of the taper. An exact solution for arbitrary slope and index difference is also presented using a piecewise analysis technique and is compared with the analytical solution. The agreement between exact piecewise and analytical ray trajectories is excellent, thus establishing the accuracy of the analytical

solution. In Chapter 4, this analysis is extended to tapered parabolic-index optical fibers which constitute a three-dimensional problem. Both meridional and skew rays are investigated and ray trajectories are presented for example cases. An important feature of both tapered waveguides and fibers is their capability to focus light signal along the direction of propagation. With this capability, applications such as optical power concentrator, image-size reducer and astigmatic image modifiers are introduced. Chapter 5 addresses the application issues of tapers. Coupling efficiencies when tapers are used to couple power from collimated-beam and Lambertian light sources are discussed. It is concluded that tapered parabolic-index fibers can provide significant improvement in power coupling efficiency of focused beam sources such as edge emitting LEDs and laser diodes to waveguides and fibers. Radiation loss of tapers when used to splice two waveguides or fibers with different core sizes is also calculated in this Chapter. Chapter 6 summarizes the main conclusions and contributions of this research and points out suggestions for further investigations.

2. Light Propagation in Graded-Index Media

In this chapter Maxwell's equations are used to derive the ray equation in a general graded-index medium. In doing so, a basic assumption is made that characteristic dimensions of the medium are many times larger than the wavelength of the electromagnetic signal. The ray equation forms the foundation for the analysis of multimode graded-index tapered planar waveguides and optical fibers to be discussed in the subsequent chapters.

2.1 Wave Equation

Let us consider a linear and isotropic dielectric medium characterized by a permittivity ε and a permeability μ. It is assumed that there are no free currents and charges in the medium. The medium is, in general, inhomogeneous with ε and μ being functions of spatial coordinates. Maxwell's equations in this medium are expressed as

$$\nabla \mathbf{x} \mathbf{H} = \varepsilon \frac{\partial \mathbf{E}}{\partial t} \tag{2.1}$$

$$\nabla \mathbf{x} \mathbf{E} = -\mu \frac{\partial \mathbf{H}}{\partial t} \tag{2.2}$$

$$\nabla . (\varepsilon \mathbf{E}) = 0 \tag{2.3}$$

$$\nabla . (\mu \mathbf{H}) = 0 \tag{2.4}$$

where **E** and **H** are electric field and magnetic field intensity vectors, respectively.

Eliminating **H** (or **E**) from Maxwell's equations and assuming $\mu = \mu_o$ for nonmagnetic media, the wave equations for **E** (and **H**) are obtained as.

$$\nabla^2 \mathbf{E} + \mu_o \varepsilon \omega^2 \mathbf{E} = -\nabla [\mathbf{E} . (\nabla \varepsilon / \varepsilon)] \tag{2.5}$$

$$\nabla^2 \mathbf{H} + \mu_o \varepsilon \omega^2 \mathbf{H} = -(\nabla \varepsilon / \varepsilon) \times (\nabla \times \mathbf{H}) \tag{2.6}$$

where the time dependence of fields has been assumed to be as $e^{i\omega t}$.

In a homogeneous medium, μ and ε are constant and the right hand sides of (2.5) and (2.6) reduce to zero. Then,

$$\nabla^2 \mathbf{E} + \mu_o \varepsilon \omega^2 \mathbf{E} = 0 \tag{2.7}$$

$$\nabla^2 \mathbf{H} + \mu_o \varepsilon \omega^2 \mathbf{H} = 0 \tag{2.8}$$

For the Cartesian components of the electric and magnetic fields the scalar wave equation holds. That is, for each Cartesian field component denoted as ψ, we have

$$\nabla^2 \psi + \mu_o \varepsilon \omega^2 \psi = 0 \tag{2.9}$$

The time-harmonic solution of the scalar wave equation is expressed as

$$\psi = \psi_o . e^{j(\omega t - \mathbf{k} \cdot \mathbf{r})} \tag{2.10}$$

where ψ_o is an amplitude constant,

$\omega = 2\pi f$ is the radian frequency,

$\mathbf{k}$ is the propagation vector, and $|\mathbf{k}| = k = \omega\sqrt{\varepsilon\mu_0}$,

$\mathbf{r}$ is the position vector.

In the general case that ε depends on $\mathbf{r}$ (inhomogeneous medium), the solution in (2.10) is no longer valid. However, if variations of ε are small over the region of one wavelength, then the solution can be approximated as a locally plane-wave with

$$\psi = \psi_o(x,y,z) . e^{j(\omega t - k_o \Phi(x,y,z))} \tag{2.11}$$

where $\Phi(x,y,z)$ is a phase function and

$k_o (= \omega\sqrt{\mu_o \varepsilon_o})$ is the propagation constant in vacuum.

2.2 Ray Equation

Assuming that (2.11) is an approximate solution of (2.9), we have

$$\nabla^2\psi + k^2\psi \approx 0 \tag{2.12}$$

Using the relationship $\nabla(e^{-jk_o\Phi}) = -jk_o e^{-jk_o\Phi}\nabla\Phi$ and the identity $\nabla(fg) = f\nabla g + g\nabla f$ and noting that $\nabla^2 = \nabla.\nabla$, (2.12) is expressed as

$$\nabla.(-j\psi_o k_o e^{-jk_o\Phi}\nabla\Phi + e^{-jk_o\Phi}\nabla\psi_o) + k^2\psi_o e^{-jk_o\Phi} = 0 \qquad (2.13a)$$

Furthermore, from the vector identity $\nabla.(f\,\mathbf{F}) = \nabla f.\mathbf{F} + f\nabla.\mathbf{F}$, we have

$$\nabla.(e^{-jk_o\Phi}\nabla\psi_o) = -jk_o e^{-jk_o\Phi}\nabla\Phi.\nabla\psi_o + e^{-jk_o\Phi}\nabla^2\psi_o \qquad (2.13b)$$

and

$$\begin{aligned}\nabla.(\psi_o e^{-jk_o\Phi}\nabla\Phi) &= \nabla(\psi_o e^{-jk_o\Phi}).\nabla\Phi + \psi_o e^{-jk_o\Phi}\nabla^2\Phi \\ &= (-jk_o\psi_o e^{-jk_o\Phi}\nabla\Phi + e^{-jk_o\Phi}\nabla\psi_o).\nabla\Phi + \psi_o e^{-jk_o\Phi}\nabla^2\Phi \qquad (2.13c)\end{aligned}$$

Combining (2.13a), (2.13b), and (2.13c), yields

$$k_o^2\left(\frac{k^2}{k_o^2} - \nabla\Phi.\nabla\Phi\right)\psi_o - jk_o(2\nabla\Phi\nabla\psi_o + \psi_o\nabla^2\Phi) + \nabla^2\psi_o = 0 \qquad (2.14)$$

In the limit of k_o approaching infinity (that is, wavelength approaching zero), equation (2.14) becomes

$$(\nabla\Phi)^2 = n^2 \qquad (2.15)$$

where $n = \dfrac{k}{k_0}$ is the refractive index of the medium. Equation (2.15) is known as the

'eikonal' equation.

A ray described by the position vector $\mathbf{r}$ is shown in Figure 2.1. If we define s as the distance measured along the ray path, the unit vector $\hat{\mathbf{s}}$ is expressed as

$$\hat{\mathbf{s}} = \frac{d\mathbf{r}}{ds} \tag{2.16}$$

By the property of the gradient of a scalar function, $\nabla\Phi$ is a vector perpendicular to the phase front surface $\Phi(x,y,z)$ = const. The unit vector $\hat{\mathbf{s}}$ may thus be expressed as

$$\hat{\mathbf{s}} = \nabla\Phi/|\nabla\Phi| = \frac{1}{n}(\nabla\Phi) \tag{2.17}$$

Equating (2.16) and (2.17), we obtain

$$n\frac{d\mathbf{r}}{ds} = \nabla\Phi \tag{2.18}$$

Taking the derivative of (2.18) with respect to s, yields

$$\frac{d}{ds}(n\frac{d\mathbf{r}}{ds}) = \frac{d}{ds}(\nabla\Phi) \tag{2.19}$$

Using the relations $d(\nabla\Phi) = (d\mathbf{r}.\nabla)(\nabla\Phi)$, where $d\mathbf{r} = dx\,\hat{a}_x + dy\,\hat{a}_y + dz\,\hat{a}_z$ and $\nabla =$

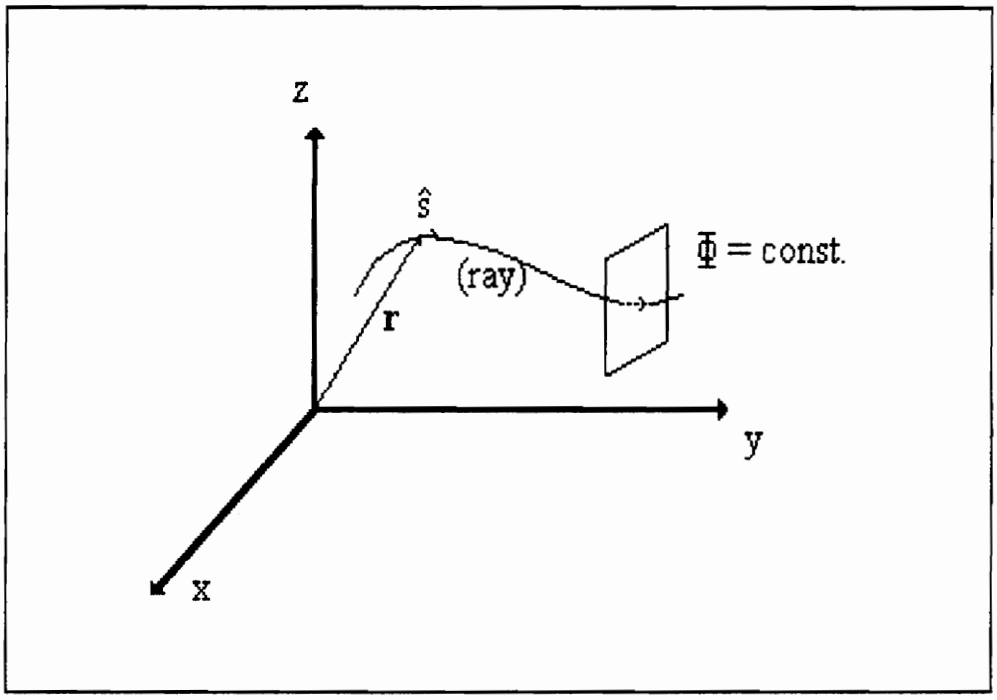

Figure 2.1 A ray described by the position vector **r**. The surface of constant phase is normal to the ray path.

$(\frac{\partial}{\partial x})\hat{a}_x + (\frac{\partial}{\partial y})\hat{a}_y + (\frac{\partial}{\partial z})\hat{a}_z$, Eq. (2.19) can be written as

$$\frac{d}{ds}(n\frac{d\mathbf{r}}{ds}) = \frac{d\mathbf{r}}{ds}.\nabla(\nabla\Phi)$$

$$= \frac{1}{n}(\nabla\Phi).\nabla(\nabla\Phi), \text{ using (2.18)}$$

$$= \frac{1}{2n}\nabla[(\nabla\Phi)^2]$$

$$= \frac{1}{2n}\nabla n^2, \text{ using (2.15)}$$

$$= \nabla n$$

Finally, we get

$$\frac{d}{ds}(n\frac{d\mathbf{r}}{ds}) = \nabla n. \tag{2.20}$$

Equation (2.20) is the desired ray equation. This equation is the basis for geometrical optics analysis of multimode waveguides and optical fibers. We use this equation to analyze transmission properties of tapered graded-index planar waveguides and optical fibers.

3. Ray Analysis of Planar Graded-Index Linear Tapers

Ray analysis of graded-index dielectric waveguides with planar boundaries is addressed. The waveguide structure is assumed to extend to infinity uniformly in both negative and positive y-directions, thus reducing the problem to a two-dimensional one. In other words, all solutions are independent of the y coordinate. First, ray trajectories in axially uniform planar guides, in which the core refractive index does not vary with z (i.e., in the direction of propagation), are studied. Attention will be focused on the case when the core region of the waveguide has a parabolic-index variation, while the cladding is homogeneous with a constant refractive index. Then, ray trajectories in tapered planar waveguides are examined. An approximate analytical solution as well as exact piecewise numerical solution are presented. The two solutions are compared and the accuracy of the analytical solution is established.

3.1 Uniform Planar Waveguides

The geometry and coordinates of a uniform graded-index planar guide are shown in Figure 3.1. For a two dimensional problem, the position vector **r** in the y=0 plane is expressed as

$$\mathbf{r} = x\,\hat{a}_x + z\,\hat{a}_z \tag{3.1}$$

Assuming that the refractive index is only a function of x, its gradient is expressed as

$$\nabla n(x) = \frac{dn}{dx}\,\hat{a}_x \tag{3.2}$$

Substituting (3.1) and (3.2) in the ray equation (2.20), we obtain

$$\frac{d}{ds}\left(n\frac{dx}{ds}\right) = \frac{dn}{dx} \tag{3.3}$$

$$\frac{d}{ds}\left(n\frac{dz}{ds}\right) = 0 \tag{3.4}$$

Integrating both sides of (3.4) yields $n\dfrac{dz}{ds} = \text{constant} = \overline{\beta}$, or

$$\frac{dz}{ds} = \frac{1}{n}\,\overline{\beta} \tag{3.5}$$

The constant coefficient $\overline{\beta}$ turns out to be the normalized axial propagation

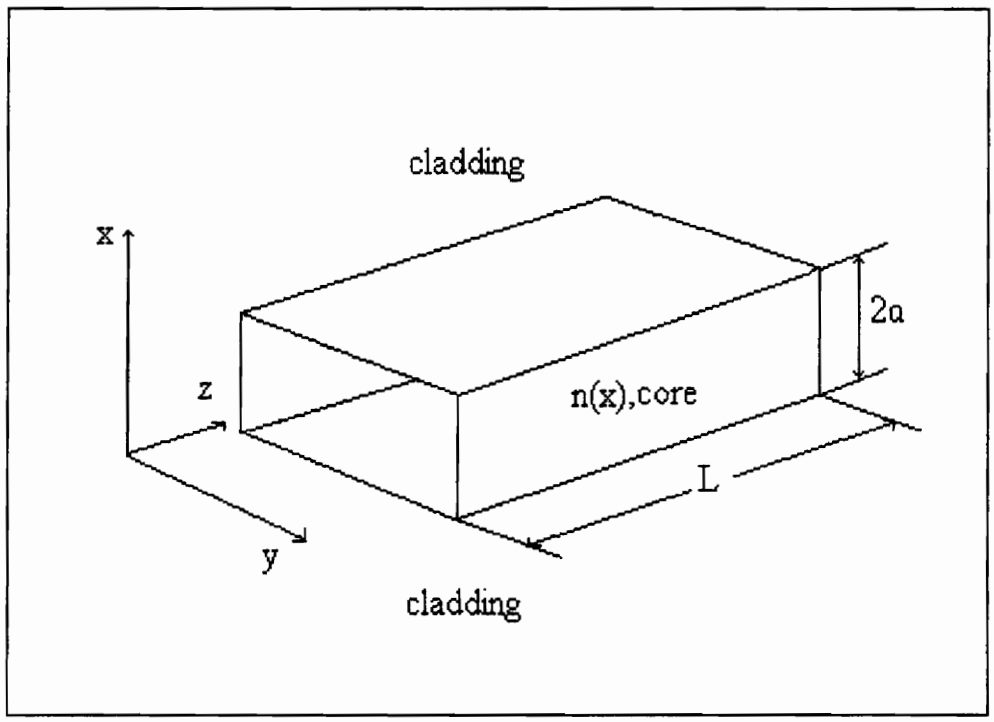

Figure 3.1 Geometry and coordinates for a uniform graded-index waveguide.

constant β / k_0. Using chain differentiation we can write

$$\frac{d}{ds} = \frac{d}{dz}\frac{dz}{ds} = \frac{\overline{\beta}}{n}\frac{d}{dz} \tag{3.6}$$

Finally, combining (3.3) and (3.6), we obtain the following result.

$$\overline{\beta}^2 \frac{d^2x}{dz^2} - \frac{1}{2}\frac{dn^2}{dx} = 0 \tag{3.7}$$

If the core of the guide is homogeneous, the refractive index n is constant, $\frac{dn^2}{dx} = 0$, and the solution of (3.7) is readily obtained as

$$x = \mathrm{A}z + \mathrm{B} \tag{3.8}$$

where A and B are constant coefficients. The result in (3.8) clearly shows that ray trajectories in a step-index waveguide are straight lines.

Next, we consider a graded-index waveguide with a parabolic index profile defined as

$$n^2(x) = \begin{cases} n_1^2\left[1 - 2\Delta\left(\frac{x}{a}\right)^2\right], & |x| < a \\ n_1(1-2\Delta), & |x| > a \end{cases} \tag{3.9}$$

where $2a$ is the thickness of the core region of the waveguide, n_1 is the refractive index of core at $x = 0$, and $\Delta = \frac{n_1^2 - n_2^2}{2n_1^2}$ is the profile height parameter.

In the $|x| < a$ region, using (3.9) in (3.7), yields

$$\frac{d^2x}{dz^2} + 2\Delta\left(\frac{n_1^2}{\bar{\beta}^2 a^2}\right)x = 0 \tag{3.10}$$

Equation (3.10) is a second-order ordinary differential equation with constant coefficients whose solution is readily expressed as

$$x = x_0 \sin\left(\frac{n_1\sqrt{2\Delta}}{\bar{\beta}}\frac{z}{a} + \varphi_o\right) \tag{3.11}$$

where x_0 and φ_0 are constants of integration and are determined from the initial ray conditions. These conditions are initial ray position and ray slope. Assuming that $x = x_1|_{z=0}$ and $\left.\frac{dx}{dz}\right|_{z=0} = \alpha_o$, yields $x_1 = x_0 \sin(\varphi_0)$ and $\alpha_0 = x_0\left(\frac{n_1\sqrt{2\Delta}}{a\bar{\beta}}\right)\cos(\varphi_0)$. Then, we obtain

$$|x_0| = \sqrt{x_1^2 + \left(\frac{\alpha_0\bar{\beta}a}{n_1\sqrt{2\Delta}}\right)^2} \tag{3.12}$$

$$\varphi_0 = \sin^{-1}\left(\frac{x_1}{x_0}\right) \tag{3.13}$$

Considering (3.11), since the absolute value of any sine or cosine function is less than or equal to one, then $|x|_{\max}$ is equal to $|x_0|$. Thus, for rays to be bound to the core region throughout the waveguide, $|x_0| \le a$ must be satisfied. Imposing this condition, yields

$$\alpha_0^2 \le \frac{n_1^2 2\Delta\left(1-\left(\frac{x_1}{a}\right)^2\right)}{\bar{\beta}^2}$$

or

$$-\frac{n_1\sqrt{2\Delta\left(a^2-x_1^2\right)}}{a\bar{\beta}} \le \alpha_0 \le \frac{n_1\sqrt{2\Delta\left(a^2-x_1^2\right)}}{a\bar{\beta}} \tag{3.14}$$

If α_0 is not in the range specified by (3.14), the ray will leak out of the core region and follows a straight-line path in the cladding region with the slope $\left.\frac{dx}{dz}\right|_{z=z_0}$,where z_0 is the leaking point, that is the point at which the ray enters into the cladding region. To find z_0, we need to calculate the smallest positive solution of $|x(z_0)| = a$. Substituting for $x(z_0)$ from (3.11), yields

$$\left| x_o \sin\left(\frac{n_1\sqrt{2\Delta}}{\bar{\beta}}\frac{z_0}{a} + \varphi_o\right)\right| = a \tag{3.15}$$

where $|x_0|$ and φ_0 are defined in (3.12) and (3.13), respectively. Solving (3.15), the smallest positive solution for z_0 is obtained as

$$z_0 = \frac{(\varphi_0' - \varphi_0)\bar{\beta}a}{n_1\sqrt{2\Delta}} \tag{3.16}$$

where

$$\varphi_0' = \sin^{-1}\left(\frac{a}{x_0}\right) = \sin^{-1}\left(\frac{1}{\sqrt{\left(\frac{x_1}{a}\right)^2 + \left(\frac{\alpha_0\bar{\beta}}{n_1\sqrt{2\Delta}}\right)^2}}\right) \tag{3.17}$$

Finally, it is clearly seen from (3.11) that the ray paths in parabolic-index planar waveguides are sinusoidal.

3.2 Ray Analysis of Graded-Index Tapered Waveguides

In this section, an analytical solution of ray equation in graded-index planar waveguide tapers is developed. The index profile of the taper is assumed to be parabolic and is described as

$$n^2(x,z) = \begin{cases} n_1^2\left[1 - 2\Delta\left(\dfrac{x}{a-\alpha z}\right)^2\right], & |x| \le a - \alpha z \\ n_2^2 = n_1^2(1-2\Delta), & |x| > a - \alpha z \end{cases} \tag{3.18}$$

where a is the thickness of the core at $z = 0$ and α is the slope of the taper. Assuming that L is the length of the taper and b is the thickness of the core at $z = L$, we have $\alpha = \dfrac{a-b}{L}$. Figure 3.2 shows the geometry, parameters and index profiles at the end faces for a parabolic index taper. The gradient of refractive index in the core of the taper is expressed as

$$\nabla n(\mathbf{r}) = -\frac{2n_1\Delta x}{(a-\alpha z)^2}\hat{a}_x - \frac{2n_1\Delta\alpha x^2}{(a-\alpha z)^3}\hat{a}_z \tag{3.19}$$

For tapers with small slopes ($\alpha << 1$), the z-component of ∇n, which is of the order $\alpha\Delta$, is much smaller than the x-component which is of the order Δ and is neglected

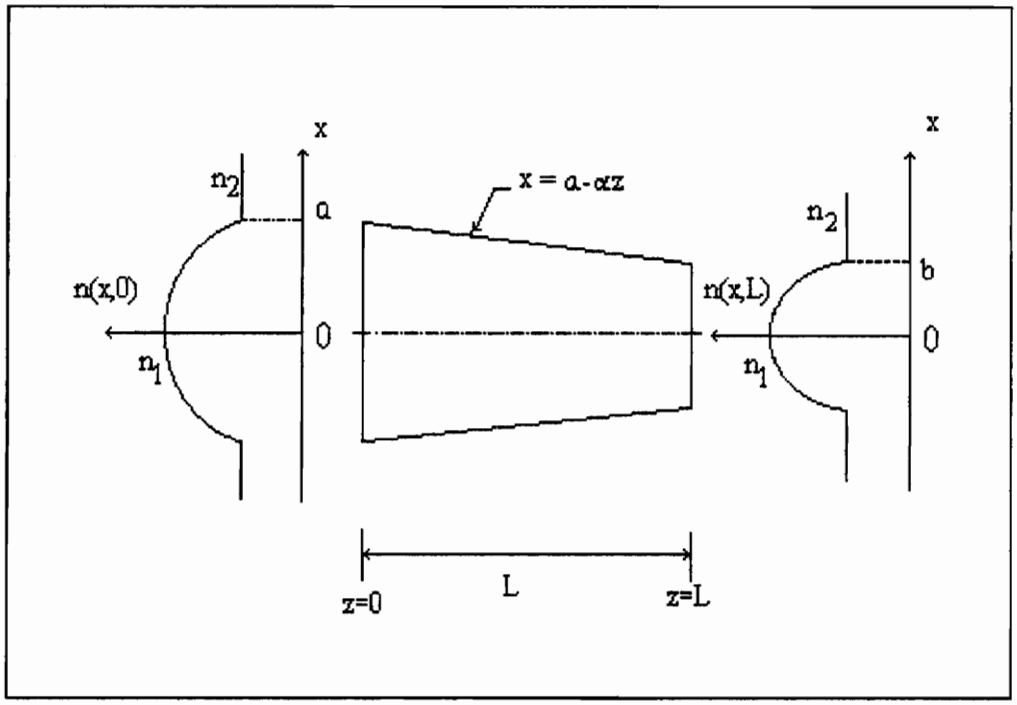

Figure 3.2 Geometry and parameters for a linearly tapered parabolic-index planar waveguide.

in determining the solution for ray trajectories. Substituting (3.1) and (3.19) in the ray equation (2.20), yields

$$\frac{d}{ds}(n\frac{dx}{ds}) = \frac{\partial n}{\partial x} = -\frac{2n_1\Delta x}{(a-\alpha z)^2} \tag{3.20}$$

$$\frac{d}{ds}(n\frac{dz}{ds}) \approx 0 \tag{3.21}$$

Integrating both sides of (3.21), $n\frac{dz}{ds} = \text{constant} = \overline{\beta}$. With the help of (3.5) and (3.6), we obtain

$$\overline{\beta}^2\frac{d^2x}{dz^2} - \frac{1}{2}\frac{\partial n^2}{\partial x} = 0 \tag{3.22}$$

Substituting for n^2 from (3.18) in (3.22), we have

$$(a-\alpha z)^2\frac{d^2x}{dz^2} + \frac{2\Delta n_1^2}{\overline{\beta}^2}x = 0 \tag{3.23}$$

Equation (3.23) is a second-order ordinary differential equation but with variable coefficients. In order to solve this equation, first a new variable $z' = \frac{a-\alpha z}{a}$ is introduced, then

$$\frac{d}{dz} = \frac{d}{dz'}\frac{dz'}{dz} = -\frac{\alpha}{a}\frac{d}{dz'}$$
$$\frac{d^2}{dz^2} = \frac{d}{dz}\left(-\frac{\alpha}{a}\frac{d}{dz'}\right) = \frac{\alpha^2}{a^2}\frac{d^2}{dz'^2}$$

and Eq. (3.23) can be rewritten as

$$z'^2 \frac{d^2x}{dz'^2} + \frac{2\Delta n_1^2}{\overline{\beta}^2 \alpha^2} x = 0 \tag{3.24}$$

We further introduce the variable t such that $z' = e^t$, then

$$\frac{d}{dz'} = \frac{d}{dt}\frac{dt}{dz'} = \frac{1}{z'}\frac{d}{dt}$$
$$\frac{d^2}{dz'^2} = \frac{d}{dz'}\left(\frac{1}{z'}\frac{d}{dt}\right) = \frac{1}{z'^2}\left[-\frac{d}{dt} + \frac{d^2}{dt^2}\right]$$

and Eq. (3.24) becomes

$$\frac{d^2x}{dt^2} - \frac{dx}{dt} + Cx = 0 \tag{3.25}$$

where $C = \frac{2\Delta n_1^2}{\overline{\beta}^2 \alpha^2}$. The solution of (3.25) is expressed as

$$\begin{aligned} x &= x_0\, e^{t/2} \sin(t.\sqrt{C - 1/4} + \varphi_o) \\ &= x_0 \sqrt{z'} \sin(\ln z'.\sqrt{C - 1/4} + \varphi_o) \\ &= x_0 \sqrt{\frac{a - \alpha z}{a}} \sin\left[\ln\left(\frac{a - \alpha z}{a}\right).\sqrt{\frac{2\Delta n_1^2}{\alpha^2 \overline{\beta}^2} - \frac{1}{4}} + \varphi_o\right] \end{aligned} \tag{3.26}$$

where x_0 and φ_0 are constants of integration and are determined by initial ray conditions.

Assuming that at $z = 0$, we have $x = x_1$ and $\frac{dx}{dz} = \alpha_o$, yields $x_1 = x_0 \sin(\varphi_0)$ and

$\alpha_0 = -\frac{x_0\alpha}{a}\left[\left(\sqrt{\frac{2\Delta n_1^2}{\alpha^2\bar{\beta}^2}-\frac{1}{4}}\right)\cos\varphi_0+\frac{1}{2}\sin\varphi_0\right]$. Then, we obtain

$$|x_0| = \sqrt{x_1^2+\frac{\left(\frac{\alpha_0 a}{\alpha}+\frac{x_1}{2}\right)^2}{\left(\frac{2\Delta n_1^2}{\bar{\beta}^2\alpha^2}-\frac{1}{4}\right)}} \tag{3.27}$$

$$\varphi_0 = \sin^{-1}\left(\frac{x_1}{x_0}\right) \tag{3.28}$$

The slope of the ray at z=0, namely α_0 in (3.23), may be expressed in terms of $\bar{\beta}$. Noting that $\alpha_0 = \tan\theta_0 = \frac{\left(1-\cos^2\theta_0\right)^{\frac{1}{2}}}{\cos\theta_0}$ and $\cos\theta_0 = \frac{dz}{ds} \approx \frac{\bar{\beta}}{n_1}$, where θ_0 is the angle between the ray path and the z-axis at z=0, we have $\alpha_0 = \frac{\left(n_1^2-\bar{\beta}^2\right)^{\frac{1}{2}}}{\bar{\beta}}$, or $\left(\frac{n_1}{\bar{\beta}}\right)^2 = 1+\alpha_0^2$.

For the special case of $x_1 = 0$, we have $\varphi_0 = 0$ and $|x_0| = \frac{2\alpha_0 a}{\sqrt{8\Delta\left(1+\alpha_0^2\right)-\alpha^2}}$.

The result in Eq. (3.26) indicates that the ray trajectories are sinusoidal function with decreasing amplitude and decreasing period. Also, Eq. (3.26) represents real rays in the core region if $\frac{2\Delta n_1^2}{\bar{\beta}^2\alpha^2}-\frac{1}{4} \geq 0$. Substituting for α, yields

$$L \geq \frac{\bar{\beta}(a-b)}{\sqrt{8\Delta n_1}} = \frac{(a-b)}{2\sqrt{2\Delta\left(1+\alpha_0^2\right)}} \tag{3.29}$$

However, if (3.29) is not satisfied, ray trajectories in the core region of the taper will be described by a hyperbolic sine function given as

$$x = \bar{x}_0 \sqrt{\frac{a - \alpha z}{a}} \sinh\left[\sqrt{\frac{1}{4} - \frac{2\Delta n_1^2}{\bar{\beta}^2 \alpha^2}} \ln\left(\frac{a - \alpha z}{a} \right) + \bar{\varphi}_0 \right] \tag{3.30}$$

where $\bar{x}_0$ and $\bar{\varphi}_0$ are constant coefficients. Such rays described by the above equation do not go through turning points and thus are not generally confined to the core region, if the taper is not so short that the rays exit the taper before they reach the core-cladding boundary. These rays are of little practical significance and are not analyzed any further. For bound rays, the condition $|x| < a - \alpha z$ must be satisfied. This condition is met if $L \le z_0$, where z_0 is the smallest positive solution of $|x(z_0)| = a - \alpha z_0$. To find the point at which $z = z_0$ where the ray reaches the cladding region and becomes a leaky ray, we substitute for $x(z_0)$ from (3.26), gives

$$\left| x_o \sin\left[\ln\left(\frac{a - \alpha z_o}{a} \right) \cdot \sqrt{\frac{2\Delta n_1^2}{\alpha^2 \bar{\beta}^2} - \frac{1}{4}} + \varphi_o \right] \right| = \sqrt{a(a - \alpha z_o)} \tag{3.31}$$

which is a transcendental equation and can be solved by numerical techniques. Taking advantage of the fact that most leaky rays cross the core-cladding boundary in the neighborhood of their turning points, an approximate solution of z_0 may be considered

as the intersection of the envelope of the ray trajectory and the core-cladding boundary. From (3.27) and $|x_0| = \sqrt{a(a - \alpha z_o)}$, we obtain

$$z_o = \frac{a}{\alpha} - \frac{\alpha_0^2 a^2 + \alpha\alpha_0 a x_1 + 2\Delta x_1^2\left(1+\alpha_0^2\right)}{a\alpha\left[2\Delta\left(1+\alpha_0^2\right) - \frac{\alpha^2}{4}\right]} \tag{3.32}$$

For weakly guiding tapers with small angles $\alpha^2 << 8\Delta << 1$, the term $\left[2\Delta\left(1+\alpha_0^2\right) - \frac{\alpha^2}{4}\right]$ is greater than zero. Using (3.32) in $L \leq z_o$, the condition for bound rays is obtained as

$$(2\Delta T - 1)\alpha_0^2 - \left(\frac{\alpha x_1}{a}\right)\alpha_0 + \left[2\Delta T - \left(\frac{b\alpha^2}{4a}\right)\right] \geq 0 \tag{3.33}$$

where

$$T = \frac{b}{a} - \left(\frac{x_1}{a}\right)^2 \tag{3.34}$$

Solving (3.33) for α_0, yields

$$\alpha_{01} \leq \alpha_0 \leq \alpha_{02} \tag{3.35}$$

where

$$\alpha_{01} = -\frac{\alpha x_1}{2aQ} - \sqrt{T\left[\frac{2\Delta}{Q} + \frac{\alpha^2\left(1 - \frac{2\Delta b}{a}\right)}{4Q^2}\right]} \tag{3.36a}$$

$$\alpha_{02} = -\frac{\alpha x_1}{2aQ} + \sqrt{T\left[\frac{2\Delta}{Q} + \frac{\alpha^2\left(1 - \frac{2\Delta b}{a}\right)}{4Q^2}\right]} \tag{3.36b}$$

with $Q = 1 - 2\Delta T$. However α_{01} and α_{02} exist only if the term in square root is equal to or greater than zero. Noting that when (3.29) is satisfied, the term in the square bracket never becomes negative, then $T \geq 0$ must be met. Using this condition in (3.34), gives

$$|x_1| \leq \sqrt{ab} \tag{3.37}$$

Equation (3.37) indicates that all rays entering the taper in the region $\sqrt{ab} < x_1 \leq a$ and $-a \leq x_1 < -\sqrt{ab}$ will leak out of the taper. With $\Delta << 1$, $T < 1$, $Q \approx 1$ and $\alpha^2 << 8\Delta << 1$, (3.35) reduces to

$$-\frac{\alpha x_1}{2a} - \sqrt{2\Delta T} \leq \alpha_0 \leq -\frac{\alpha x_1}{2a} + \sqrt{2\Delta T} \tag{3.38}$$

When specific initial ray conditions α_0 and x_1 are given, the minimum taper length may be calculated using (3.33).

3.3 Exact Numerical Analysis of Graded-Index Taper

In order to examine the accuracy of the approximate analytical solution obtained in the previous section, an exact solution of ray trajectories in graded-index tapers is discussed using a piecewise numerical technique. Figure 3.3a illustrates the geometry and coordinates for a segmented waveguide. The graded-index taper is divided into N segments, and each segment is considered as a uniform waveguide of length

$\frac{L}{N}$. Figure 3.3b shows the geometry and coordinates for an ith segment of the taper. For the ith segment, we have

$$z_i = (i-1).\frac{L}{N} \quad ; i = 1,2,\ldots N \tag{3.39}$$

$$z' = z - z_i \tag{3.40}$$

$$z_{i+1} = i.\frac{L}{N} \quad ; i = 1,2,\ldots N \tag{3.41}$$

$$a_i = a - \alpha.(i-1).\frac{L}{N} \quad ; i = 1,2,\ldots N \tag{3.42}$$

Using the result in (3.11), the solution of ray equation in the i th segment can be written as

$$x = x_{oi} \sin\left(\frac{n_1\sqrt{2\Delta}}{\bar{\beta}_i}\frac{z'}{a_i} + \varphi_{oi}\right), \; 0 < z' < \frac{L}{N} \tag{3.43}$$

The constant coefficients x_{oi} and φ_{oi} are determined from the ray slope and ray amplitude at $z' = 0$. In doing so, we proceed as follows. Differentiate equation (3.43), yields

$$\frac{dx}{dz'} = x_{oi}\left(\frac{n_1\sqrt{2\Delta}}{\bar{\beta}_i.a_i}\right)\cos\left(\frac{n_1\sqrt{2\Delta}}{\bar{\beta}_i}\frac{z'}{a_i} + \varphi_{oi}\right), \; 0 < z' < \frac{L}{N} \tag{3.44}$$

The initial conditions are expressed as

$$\left.\begin{aligned} x &= x_i \\ \frac{dx}{dz'} &= \alpha_i \end{aligned}\right\} \text{ at } \; z' = 0 \tag{3.45}$$

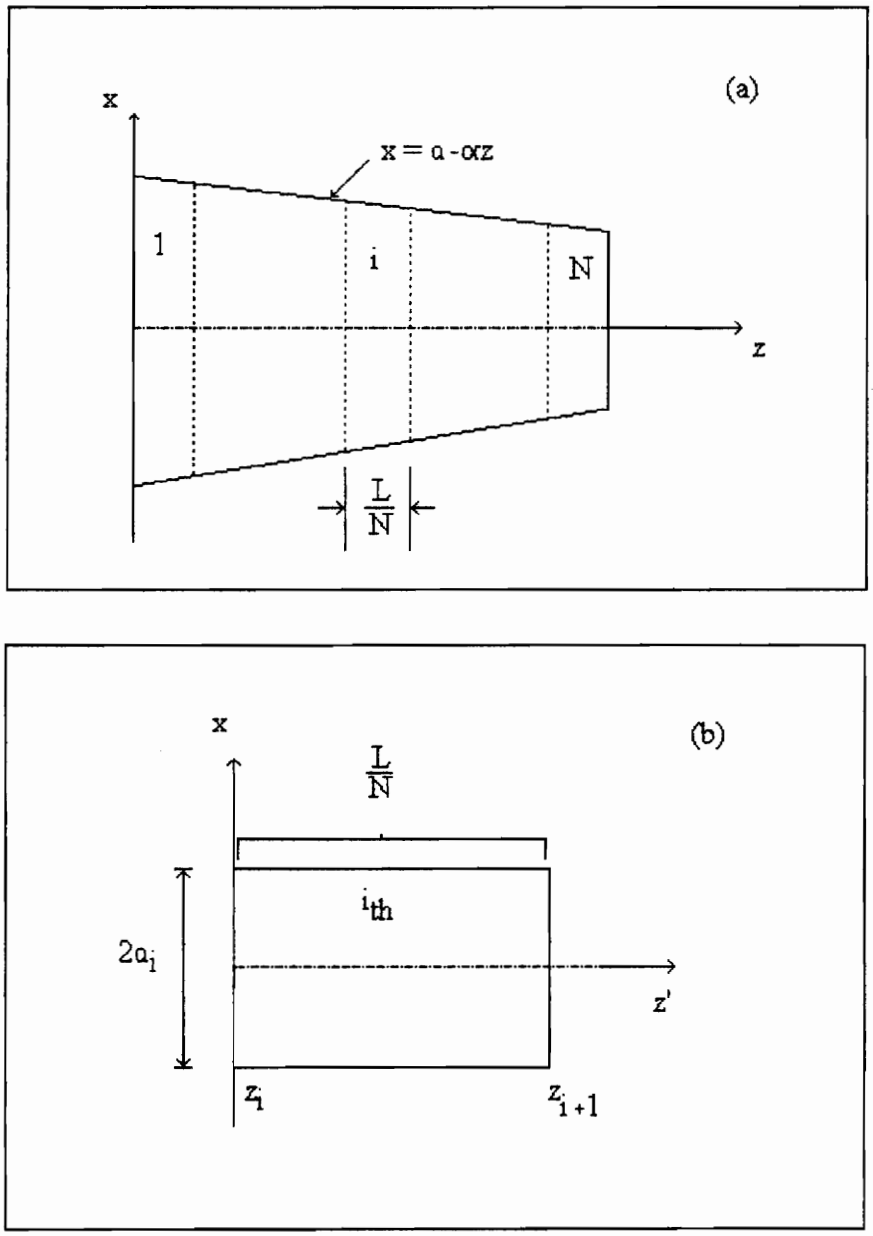

Figure 3.3 Geometry and coordinates for (a) segmented tapered graded-index waveguide, (b) *i* th segment of the taper.

Using these initial conditions in (3.43) and (3.44), we obtain

$$x_i = x_{oi} \sin \varphi_{oi} \tag{3.46}$$

$$\alpha_i = x_{oi} \left(\frac{n_1 \sqrt{2\Delta}}{\bar{\beta}_i a_i}\right) \cos(\varphi_{oi}) \tag{3.47}$$

Dividing (3.46) by (3.47), yields

$$\tan \varphi_{oi} = \frac{x_i}{\alpha_i} \left(\frac{n_1 \sqrt{2\Delta}}{\bar{\beta}_i a_i}\right) \tag{3.48}$$

But the constant $\bar{\beta}_i$ is related to α_i. To find this relationship, referring to the coordinate system and path elements along a ray trajectory, as indicated in Figure 3.4, we can write

$$\frac{dz'}{ds} = \frac{dz}{ds} = \frac{\bar{\beta}_i}{n(x_i, z_i)} = \cos\theta_i$$

$$\alpha_i = \tan\theta_i = \frac{\sin\theta_i}{\cos\theta_i} = \frac{\sqrt{1 - \cos^2\theta_i}}{\cos\theta_i}$$

$$= \sqrt{\frac{1}{\cos^2\theta_i} - 1} = \sqrt{\frac{n^2(x_i, z_i)}{\bar{\beta}_i} - 1}$$

$$\bar{\beta}_i = \frac{n(x_i, z_i)}{\sqrt{1 + \alpha_i^2}} \tag{3.49}$$

where

$$n(x_i, z_i) = n_1 \left[1 - \Delta \left(\frac{x_i}{a - \alpha z_i}\right)^2\right] \tag{3.50}$$

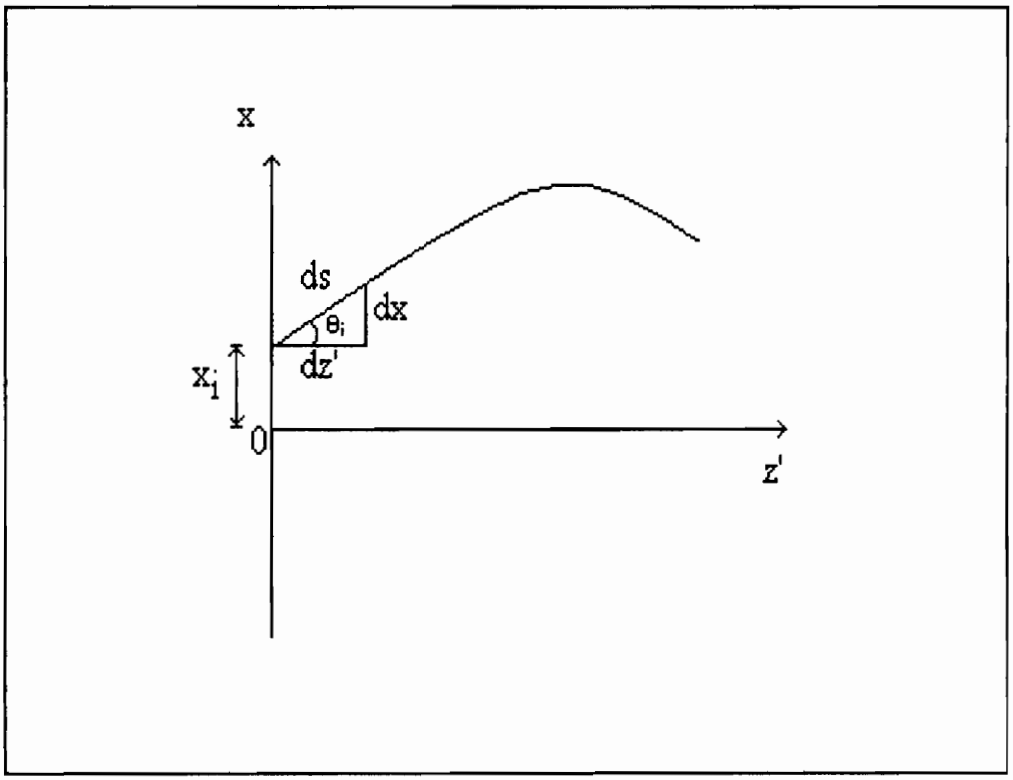

Figure 3.4 Coordinate system and path elements along a ray trajectory.

Substituting (3.49) in (3.48), we obtain

$$\tan \varphi_{oi} = \frac{x_i}{\alpha_i}\left(\frac{n_1\sqrt{2\Delta(1+\alpha_i^2)}}{a_i n(x_i,z_i)}\right) \tag{3.51}$$

$$\varphi_{oi} = \tan^{-1}\left[\frac{x_i}{\alpha_i}\left(\frac{n_1\sqrt{2\Delta(1+\alpha_i^2)}}{a_i n(x_i,z_i)}\right)\right] \tag{3.52}$$

Using (3.46) and replacing (3.40), (3.49) in (3.43), yields

$$x = \left(\frac{x_i}{\sin\varphi_{oi}}\right)\sin\left[\frac{n_1\sqrt{2\Delta(1+\alpha_i^2)}}{a_i n(x_i,z_i)}(z-z_i)+\varphi_{oi}\right], \quad z_i < z < z_{i+1} \tag{3.53}$$

The next step is to find the initial conditions for the ray in the $(i+1)$th segment.

Substituting $(z-z_i)=\frac{L}{N}$ in (3.53), gives

$$x_{i+1} = \left(\frac{x_i}{\sin\varphi_{oi}}\right)\sin\left[\frac{n_1\sqrt{2\Delta(1+\alpha_i^2)}}{a_i n(x_i,z_i)}\frac{L}{N}+\varphi_{oi}\right] \tag{3.54}$$

Combining (3.44), (3.46), (3.49), we get

$$\begin{aligned}\alpha_{i+1} &= \left.\frac{dx}{dz'}\right|_{z'=\frac{L}{N}} \\ &= \left(\frac{x_i}{\sin\varphi_{oi}}\right).\left(\frac{n_1\sqrt{2\Delta(1+\alpha_i^2)}}{a_i n(x_i,z_i)}\right)\cos\left[\left(\frac{n_1\sqrt{2\Delta(1+\alpha_i^2)}}{a_i n(x_i,z_i)}\right)\frac{L}{N}+\varphi_{oi}\right]\end{aligned} \tag{3.55}$$

where $n(x_i,z_i)$ and φ_{oi} have already been defined in (3.50) and (3.52), respectively. To calculate the complete solution, Eq. (3.53) is iterated in each part, from the first part to the Nth part, by using the appropriate initial conditions defined in (3.52),

(3.54) and (3.55). However, the initial conditions for the first part, x_1 and α_1 must be chosen.

3.4 Numerical Results and Accuracy of Analytical Solution

In this section, results from approximate analytical and exact numerical solutions are discussed and compared for several example cases. First, a taper with parameter a=100 μm, b=25 μm, L=1cm, n_1=1.5, n_2=1.48 is considered. For this taper, Figures (3.6)-(3.8) illustrate trajectories for α_0=0.0517, 0.0816 and 0.1004. For x_1= 0, the condition for rays to be bound to the core is $|\alpha_0| \le 0.0816 = \alpha_{0,\max}$. Thus, for α_0=0.0517 and 0.0816, the rays are fully bound and critically bound to the core as indicated in Figures 3.6 and 3.7, respectively. However, for α_0=0.1004 which is greater than $\alpha_{0,\max}$, the ray is leaky as shown in Figure 3.8. It is observed that the ray in Figure 3.8 becomes leaky at z_0=8.75 mm. Using (3.32), an approximate value of 8.32 mm is obtained for z_0 which is reasonably accurate. Figures (3.6)-(3.8) also compare ray trajectories calculated from approximate analytical and exact numerical solutions. As noted, the agreement between the approximate and exact rays is excellent, indicating that for $\alpha << 1$ and $\Delta << 1$ (in this example $\alpha = \dfrac{100-25}{10{,}000} = 0.0075$ and $\Delta = \dfrac{1.5^2 - 1.48^2}{2 \times 1.5^2} = 0.013244$) the analytical solution presented in Section3.2 predicts the transmission properties of the graded-index taper very accurately.

Next, we consider an example for which one of the conditions $\alpha << 1$ and $\Delta << 1$ is relaxed in order to see how well the exact and approximate solutions agree. We consider a taper with a=100 μm, b=25 μm, L=1cm, n_1=1.5, n_2=1. This is an extreme case of a taper with no cladding and $\Delta = 0.278$. Figure 3.9a compares exact and approximate ray trajectories for a ray with a slope of α_0=0.1 at the beginning of the taper. This ray remains bound to the core throughout the length of the taper, since from (3.38) $\alpha_{0,\max}$ = 0.2357 which is greater than α_0. It is noted that for $z < 5$ mm, the agreement between the exact and approximate ray trajectories is excellent and the two rays are nearly indistinguishable. For $5 < z < 10$ mm, however, the difference between the two rays becomes noticeable and grows larger for larger values of z. To see this difference at larger values of z more clearly, a portion of Figure 3.9a is expanded as illustrated in Figure 3.9b. It is emphasized that, even in such an extreme case (which is of little practical interest), the analytical solution is sufficiently accurate for rays which are well confined to the core. In summary, the approximate analytical analysis accurately predicts transmission properties of weakly guiding ($\Delta << 1$) graded-index tapers with small angles ($\alpha << 1$).

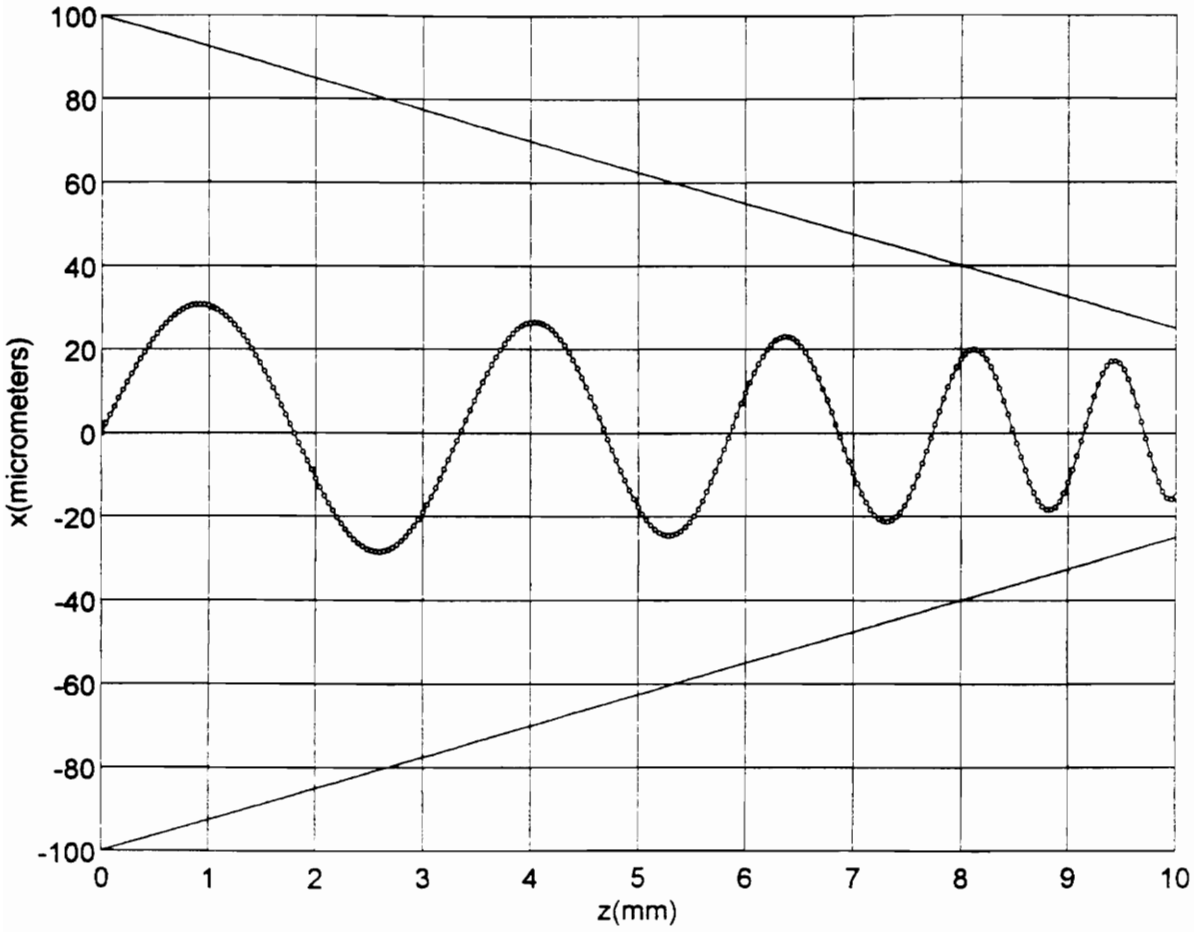

Figure 3.6 Ray trajectories in a taper with a=100 μm, b=25 μm, L=1cm, n_1=1.5, n_2= 1.48, for a bound ray with α_0=0.0517; (∘∘∘) exact, (- - -) approximate.

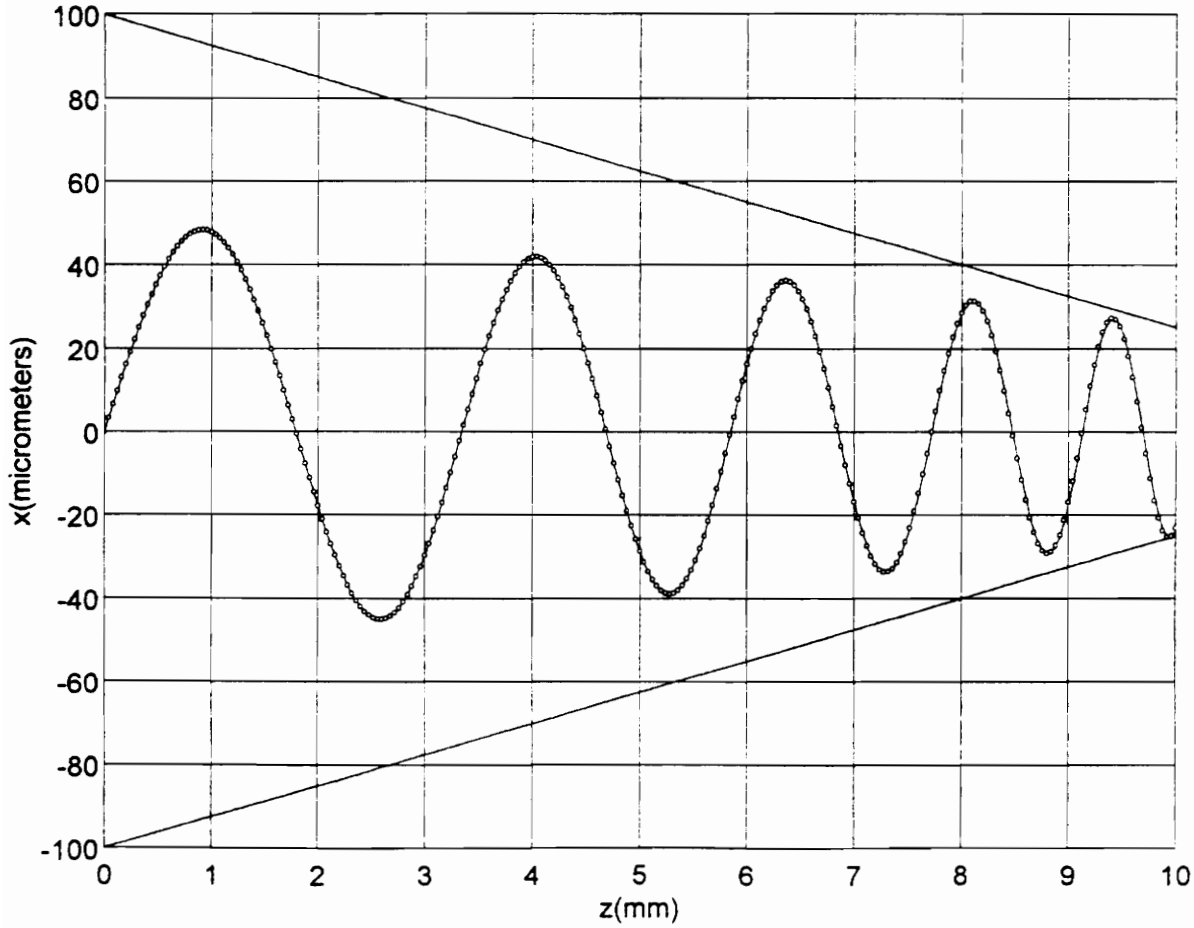

Figure 3.7 Ray trajectories in a taper with a=100 μm, b=25 μm, L=1cm, n_1=1.5, n_2= 1.48, for a ray with $\alpha_{0,\max}$=0.0816 which is critically bound to the core; (∘∘∘) exact, (- - -) approximate.

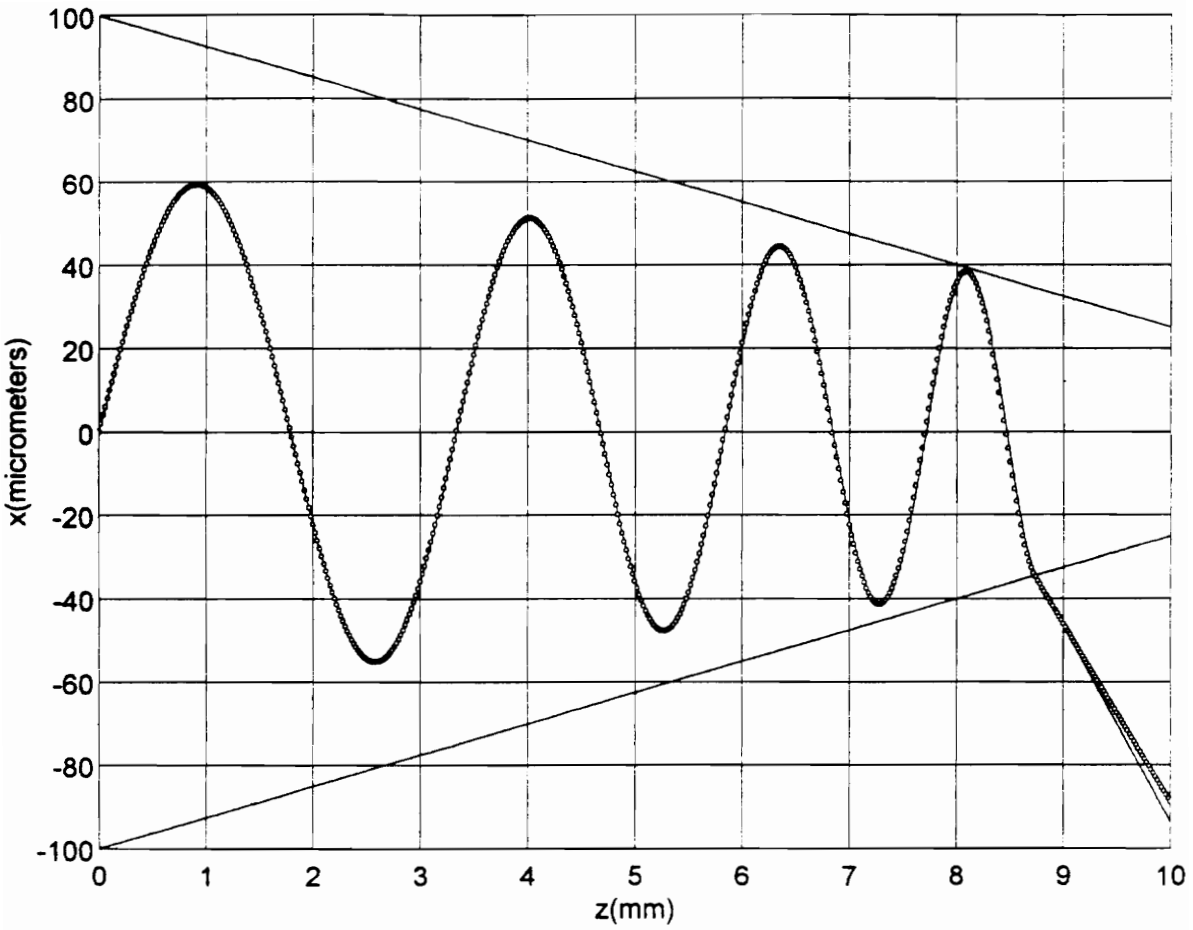

Figure 3.8 Ray trajectories in a taper with a=100 μm, b=25 μm, L=1cm, n_1=1.5, n_2= 1.48, for a leaky ray with α_0=0.1004; (∘∘∘) exact, (- - -) approximate.

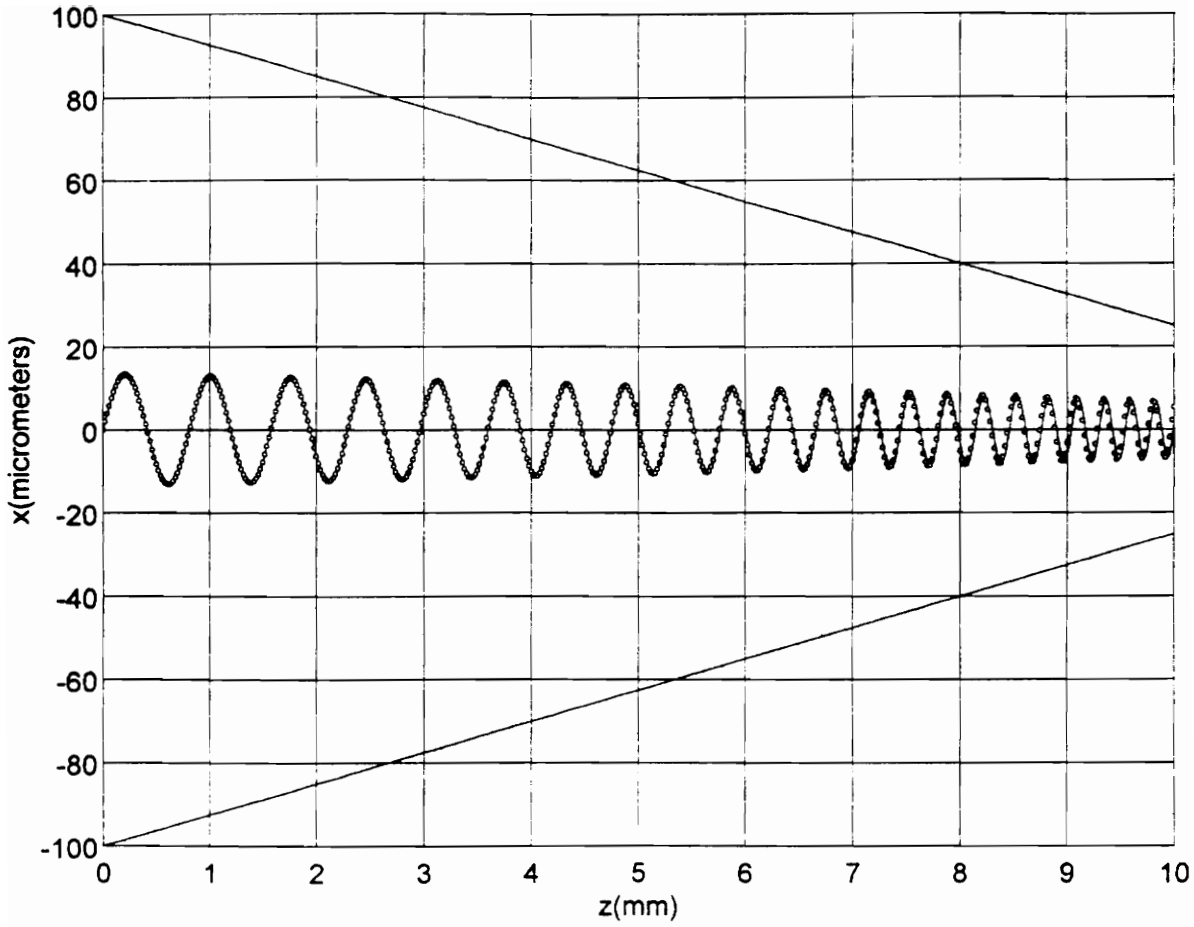

Figure 3.9a Ray trajectories in a taper with a=100 μm, b=25 μm, L=1cm, n_1=1.5, n_2=1 (no cladding), for a bound ray with α_0=0.1; (∘∘∘) exact, (- - -) approximate.

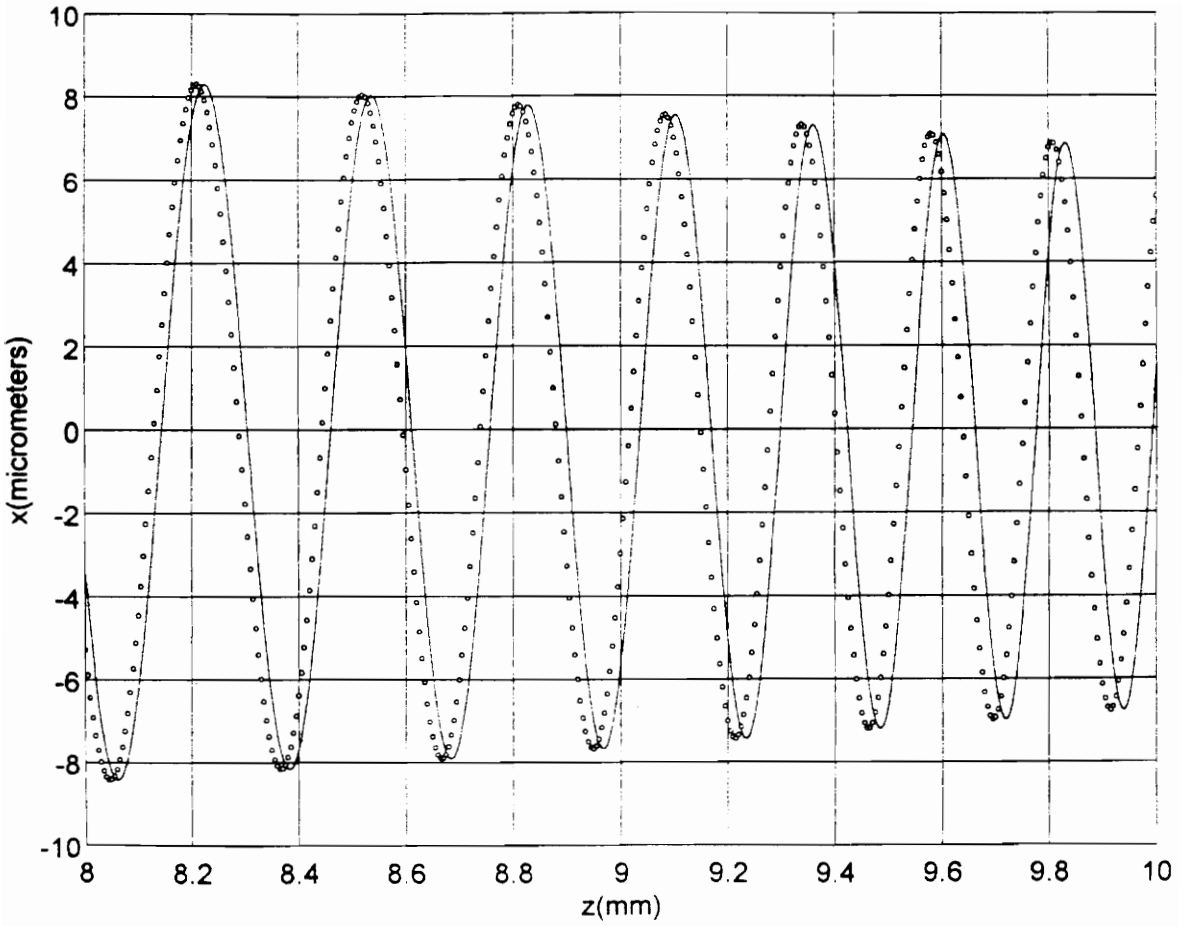

Figure 3.9b Expansion of Figure 3.9a for $8\,\text{mm} < z < 10\,\text{mm}$.

4. Ray Analysis of Graded-Index Optical Fiber Tapers

Ray analysis of tapered planar waveguides with parabolic-index profiles revealed that as light propagates towards the smaller end of taper, its power gradually concentrates along the taper. This analysis is extended here to tapered parabolic-index optical fibers. While the planar waveguide may serve as a two-dimensional model of the fiber when meridional rays are concerned, the study of skew rays requires a full three-dimensional analysis. The basic assumptions made for the analysis of the fiber taper are the same as those used in the analysis of planar waveguide taper; namely, the slope of the taper and the index difference between the core and the cladding are much smaller than unity and the radius of the core at the smaller end of the taper is many times larger than the wavelength of light. The latter assumption is essential to the validity of the geometrical optic analysis of the taper.

4.1 Uniform Parabolic-Index Fibers

Before embarking upon the analysis of tapered graded-index optical fibers, the heighlights of ray analysis for uniform multimode fibers are reviewed. This review not only prepares the ground for the ray analysis of tapered fibers, but some of the results are also needed in the calculation of radiation loss when tapers are used to splice two dissimilar core fibers. The geometry of a uniform parabolic-index fiber is shown in Figure 4.1. For the fiber geometry we have to solve the ray equation in a cylindrical polar coordinate system (r, φ, z). In this system, the position vector $\mathbf{r}$ is expressed as

$$\mathbf{r} = r\hat{a}_r + z\hat{a}_z \tag{4.1}$$

We assume that the refractive index is only a function of radial coordinate r, with no variations with φ and z and can be expressed as

$$n^2(r) = \begin{cases} n_1^2\left[1 - 2\Delta\left(\dfrac{r}{a}\right)^2\right], & r \le a \\ n_2^2 = n_1^2(1-2\Delta), & r \ge a \end{cases} \tag{4.2}$$

Putting (4.1) in the ray equation (2.20) and considering n as a function of r only, yields

$$\frac{d}{ds}\left[n(r)\frac{d}{ds}(r\hat{a}_r)\right] + \frac{d}{ds}\left[n(r)\frac{dz}{ds}\right]\hat{a}_z = \frac{dn(r)}{dr}\hat{a}_r \tag{4.3}$$

Using $\dfrac{d(\hat{a}_r)}{ds} = \dfrac{d\varphi}{ds}\hat{a}_\varphi$ and $\dfrac{d(\hat{a}_\varphi)}{ds} = -\dfrac{d\varphi}{ds}\hat{a}_r$, [29], and equating the like components, (4.3)

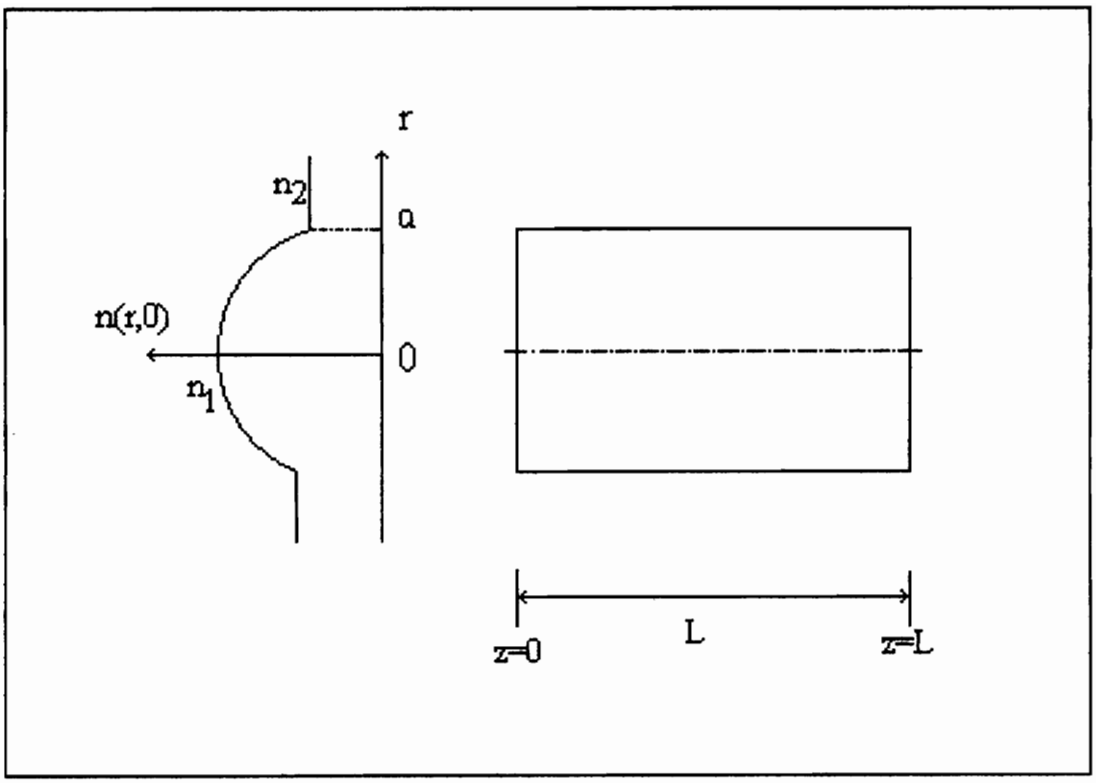

Figure 4.1 Geometry and parameters for a uniform parabolic-index fiber.

resolves into three scalar equations expressed as

$$\frac{d}{ds}\left[n(r)\frac{dz}{ds}\right]=0 \tag{4.4}$$

$$\frac{d}{ds}\left[n(r)\frac{d\varphi}{ds}\right]+\frac{2}{r}n(r)\frac{d\varphi}{ds}\cdot\frac{dr}{ds}=0 \tag{4.5}$$

$$\frac{d}{ds}\left[n(r)\frac{dr}{ds}\right]-rn(r)\left(\frac{d\varphi}{ds}\right)^2=\frac{dn(r)}{dr} \tag{4.6}$$

Equation (4.4) is the same as (3.4) for the planar guide. The solution to this equation is expressed as

$$n(r)\frac{dz}{ds}=\bar{\beta} \tag{4.7}$$

where $\bar{\beta}$ is a constant. From our experience with the graded-index planar guide, we predict that $\bar{\beta}$ is the normalized propagation constant $\bar{\beta}=\frac{\beta}{k_0}$.

The solution of (4.5), after expressing this equation as $\frac{d}{ds}\left[r^2\left(n(r)\frac{d\varphi}{ds}\right)\right]=0$ is written as

$$r^2n(r)\frac{d\varphi}{ds}=\ell_0 \tag{4.8}$$

where ℓ_0 is a constant. Using (4.7) and (4.8) in (4.6), and noting that $\frac{d}{ds}=\frac{\bar{\beta}}{n(r)}\frac{d}{dz}$ we obtain

$$\bar{\beta}^2\frac{d^2r}{dz^2}-\frac{\ell_0^2}{r^3}=\frac{1}{2}\frac{dn^2(r)}{dr} \tag{4.9}$$

The solution for ray trajectories are obtained by integrating (4.8) and (4.9). The results are:

$$z = \overline{\beta}\int_{r_0}^{r}\left[n^2(r) - \overline{\beta}^2 - \frac{\ell_0^2}{r^2}\right]^{-\frac{1}{2}} dr \tag{4.10}$$

$$\varphi = \frac{\ell_0}{\overline{\beta}}\int_{z_0}^{z}\frac{dz}{r^2(z)} \tag{4.11}$$

For the parabolic-index fiber with an index profile described by (4.2), evaluation of (4.10) and (4.11) results in, [29]

$$r = \left[\frac{r_1^2 + r_2^2}{2} - \frac{r_2^2 - r_1^2}{2}\cos\left(\frac{2V}{\beta a^2}z\right)\right]^{\frac{1}{2}} \tag{4.12}$$

$$\varphi = \frac{1}{2}\cos^{-1}\left(\frac{U^2r^2 - 2a^2\ell^2}{r^2\sqrt{U^4 - 4V^2\ell^2}}\right) \tag{4.13}$$

where

$$r_1 = \frac{a\sqrt{U^2 - \sqrt{U^4 - 4\ell^2V^2}}}{V\sqrt{2}} \tag{4.14}$$

$$r_2 = \frac{a\sqrt{U^2 + \sqrt{U^4 - 4\ell^2V^2}}}{V\sqrt{2}} \tag{4.15}$$

with $V = \sqrt{a^2k_0^2n_1^2 2\Delta}$, $U = k_0a\sqrt{n_1^2 - \overline{\beta}^2}$, and $\ell = k_0\ell_0$.

Finally, using the transverse resonance condition, it can be shown that for propagating rays the following relation must be satisfied, [29]

$$U^2 = 2V(2m + \ell + 1) \tag{4.16}$$

where ℓ=0, 1, 2, ... and m = 1, 2, 3, ... in fact represent mode numbers for $LP_{\ell m}$ modes. From (4.16), the propagation constant $\overline{\beta}$ can be calculated. When ℓ=0, it can be concluded that $\phi = \frac{\pi}{2}$, i.e. the rays are of meridional type, r_1=0, i.e. no inner caustics (consistent with the fact that rays are meridional), and $r = r_2 \sin\left(\frac{V}{\beta a^2} z\right)$. On the other hand, when $\ell \geq 1$ the rays are of skew type following helical elliptical paths along the fiber. The projection of a ray path onto a plane normal to the fiber axis is an ellipse.

4.2 Parabolic-Index Tapers

The refractive index of a linearly tapered parabolic-index fiber is expressed as

$$n^2(r,z) = \begin{cases} n_1^2\left[1 - 2\Delta\left(\frac{r}{a - \alpha z}\right)^2\right], & r \leq a - \alpha z \\ n_2^2 = n_1^2(1 - 2\Delta), & r \geq a - \alpha z \end{cases} \tag{4.17}$$

where $\Delta = \frac{n_1^2 - n_2^2}{2n_1^2} \approx \frac{n_1 - n_2}{n_1} << 1$ is the index profile height, n_1 is the index on the axis of the taper, n_2 is the index of the cladding region, and $\alpha = \frac{a - b}{L} << 1$ is the slope of the taper. Figure 4.2 shows the geometry, index profile, and parameters of the taper. Again, substituting for the position vector **r** given in (4.1) in the ray equation (2.20) and resolving it into three scalar equations, we have

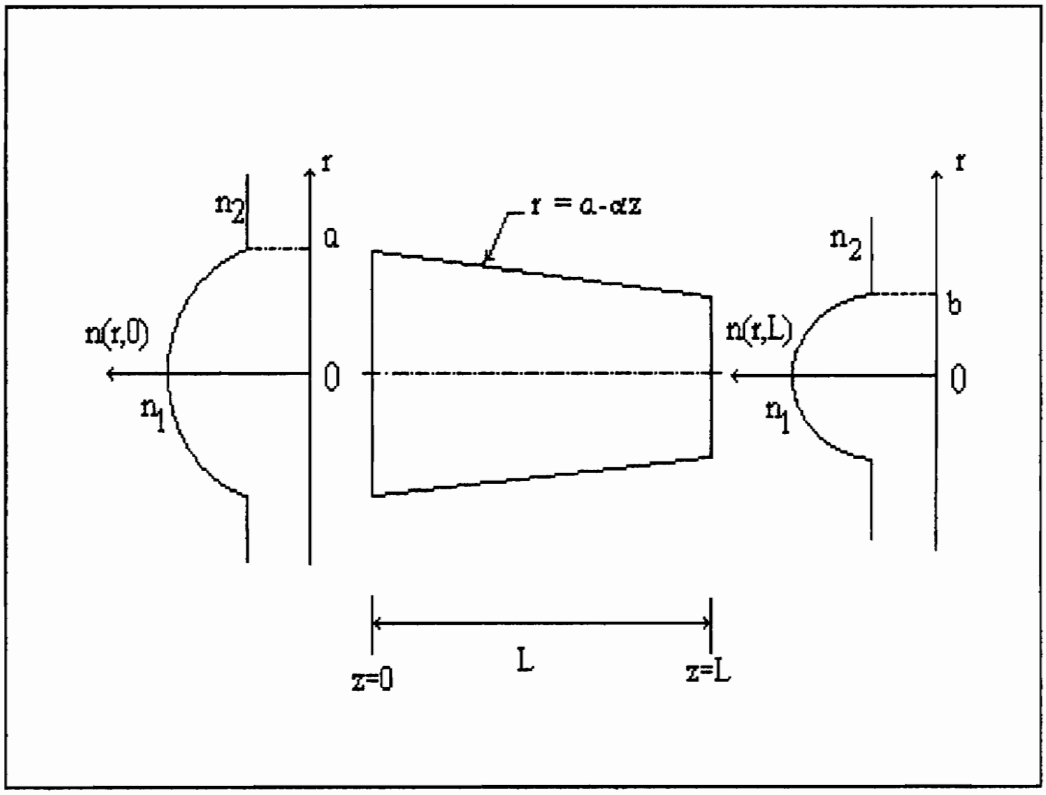

Figure 4.2 Geometry and parameters for tapered parabolic-index fiber.

$$\frac{d}{ds}\left[n(\mathbf{r})\frac{dz}{ds}\right]=\frac{\partial n(\mathbf{r})}{\partial z} \tag{4.18}$$

$$\frac{d}{ds}\left[n(\mathbf{r})\frac{dr}{ds}\right]-rn(\mathbf{r})\left(\frac{d\varphi}{ds}\right)^2=\frac{\partial n(\mathbf{r})}{\partial r} \tag{4.19}$$

$$\frac{d}{ds}\left[n(\mathbf{r})\frac{d\varphi}{ds}\right]+\frac{2}{r}n(\mathbf{r})\frac{d\varphi}{ds}\cdot\frac{dr}{ds}=\frac{1}{r}\cdot\frac{\partial n(\mathbf{r})}{\partial\varphi} \tag{4.20}$$

For the taper under investigation $n(\mathbf{r})=n(r,z)$; that is, the refractive index is independent of φ. Hence, $\frac{\partial n(\mathbf{r})}{\partial\varphi}=0$ and the right-hand side of (4.20) is zero. The gradient of $n(\mathbf{r})=n(r,z)$ is obtained as

$$\nabla n(r,z)=-2n_1\left[\Delta\left(\frac{r}{(a-\alpha z)^2}\right)\hat{a}_r-\alpha\Delta\frac{r^2}{(a-\alpha z)^3}\hat{a}_z\right],\quad r\le a-\alpha z \tag{4.21}$$

We note that $\frac{\partial n(r,z)}{\partial r}=O(\Delta)$, while $\frac{\partial n(r,z)}{\partial z}=O(\alpha\Delta)$, thus with $\alpha<<1$ it is concluded that $\frac{\partial n(r,z)}{\partial z}<<\frac{\partial n(r,z)}{\partial r}$ and the right-hand side of (4.18) is approximately zero. Using $\frac{\partial n(r,z)}{\partial z}\approx 0$ in (4.18). We have

$$\frac{d}{ds}\left[n(r,z)\frac{dz}{ds}\right]\approx 0 \tag{4.22}$$

or

$$n(r,z)\frac{dz}{ds}=\eta \tag{4.23}$$

where η is a constant. In reality, η is a slowly varying function of z, $\eta=\eta(z)$, and

represents the normalized propagation constant. That is, $\eta = \frac{\beta(z)}{k_o}$; $k_o = \frac{2\pi}{\lambda}$ with λ being the wavelength of light. For bound rays (guided modes), η is limited to the range $n_2 < \eta < n_1$ and since $n_1 \approx n_2$ ($\Delta << 1$) the approximately constant nature of η is apparent. For meridional rays, η = constant can be used without any problem. For skew ray, however, more caution is required. This point is further elaborated upon when skew rays are analyzed. From (4.23) and using chain differentiation, we have

$$\frac{d}{ds} = \frac{d}{dz}\frac{dz}{ds} = \frac{\eta}{n(r,z)}\frac{d}{dz} \tag{4.24}$$

From (4.20) with $\frac{\partial n(r,z)}{\partial \varphi} = 0$, we further obtain

$$\frac{d}{ds}\left[r^2\left(n(r,z)\frac{d\varphi}{ds}\right)\right] = 0 \tag{4.25}$$

Integrating both sides of (4.25), yields

$$r^2\left(n(r,z)\frac{d\varphi}{ds}\right) = \ell_0 \tag{4.26}$$

or

$$\frac{d\varphi}{ds} = \frac{\ell_0}{r^2 n(r,z)} \tag{4.27}$$

where ℓ_0 is a constant. Using (4.24) and (4.27) in (4.19), yields

$$\eta\frac{d}{dz}\left(\eta\frac{dr}{dz}\right) - \frac{\ell_0^2}{r^3} = \frac{1}{2}\frac{\partial n^2(r,z)}{\partial r} \tag{4.28}$$

4.2.1 Meridional Rays $(\ell_0 = 0)$

When $\ell_0 = 0$, from (4.27) it is concluded that φ = constant. However, φ = constant is a half-plane containing the z-axis. Thus, meridional rays which lie on φ = constant planes cross the z-axis(taper axis). With $\ell_0 = 0$, equation (4.28) reduces to

$$\eta \frac{d}{dz}\left(\eta \frac{dr}{dz}\right) = \frac{1}{2}\frac{\partial n^2(r,z)}{\partial r} \tag{4.29}$$

Putting $\frac{\partial n^2(r,z)}{\partial r} = -4n_1^2\Delta\frac{r}{(a-\alpha z)^2}$ and $\eta\frac{d}{dz}\left(\eta\frac{dr}{dz}\right) \approx \eta_0^2\frac{d^2r}{dz^2}$ in (4.29), we obtain

$$(a-\alpha z)^2\frac{d^2r}{dz^2} + \frac{2\Delta n_1^2 r}{\eta_0^2} = 0 \tag{4.30}$$

where η_0 is the ray constant at the beginning of the taper and is related to the slope of the ray as we have discussed in (3.22), then

$$\eta_0 = \frac{n(r,0)}{\sqrt{1+\alpha_0^2}} \tag{4.31}$$

where α_0 is the slope of the ray at $z = 0$. Equation (4.30) is identical in format to (3.23) for a planar waveguide. Thus, the solution of (4.30) is readily expressed as

$$r = r_0\sqrt{\frac{a-\alpha z}{a}}\sin\left[\sqrt{\frac{2\Delta n_1^2}{\alpha^2\eta_0^2} - \frac{1}{4}}\ln\left(\frac{a-\alpha z}{a}\right) + \theta_0\right] \tag{4.32}$$

where r_0 and θ_0 are constants and are obtained from initial ray conditions. Assuming that $r(z=0) = r_1$ and $\left.\frac{dr}{dz}\right|_{z=0} = \alpha_0$, θ_0 and r_0 are determined as

$$r_0 = \nu \sqrt{r_1^2 + \frac{\left(\frac{\alpha_0 a}{\alpha} + \frac{r_1}{2}\right)^2}{\left(\frac{2\Delta n_1^2}{\beta^2 \alpha^2} - \frac{1}{4}\right)}} \tag{4.33}$$

$$\theta_0 = \sin^{-1}\left(\frac{r_1}{r_0}\right) \tag{4.34}$$

where $\nu = +1$ or -1 such that $r \geq 0$ for all values of z.

4.2.2 Skew Rays ($\ell_0 \neq 0$)

To determine the solution for ray equation, we use the relationship $ds^2 = dr^2 + (rd\varphi)^2 + dz^2$ in conjunction with (4.23) and (4.27)

$$\begin{aligned} 1 &= \left(\frac{dr}{ds}\right)^2 + \left(\frac{rd\varphi}{ds}\right)^2 + \left(\frac{dz}{ds}\right)^2 \\ &= \left(\frac{dr}{dz}\cdot\frac{dz}{ds}\right)^2 + \left(\frac{rd\varphi}{ds}\right)^2 + \left(\frac{dz}{ds}\right)^2 \\ &= \left(\frac{\eta}{n}\cdot\frac{dr}{dz}\right)^2 + \left(\frac{\ell_0}{nr}\right)^2 + \left(\frac{\eta}{n}\right)^2 \end{aligned} \tag{4.35}$$

or

$$\eta^2\left(\frac{dr}{dz}\right)^2 = n^2 - \eta^2 - \frac{\ell_0^2}{r^2} \tag{4.36}$$

It is emphasized that (4.36) is not independent from (4.28). It is preferable to use (4.36) since it can be solved more easily. Here, while $\eta \approx$ constant can be used in the term $\eta^2\left(\frac{dr}{dz}\right)^2$, the same approximation in the right-hand-side of (4.36) should be examined

more carefully. Variations of η with respect to z may be obtained in the following form.

$$\eta^2 = n_1^2 - (n_1^2 - \eta_0^2)\frac{a}{a - \alpha z} \tag{4.37}$$

To derive (4.37), the characteristic equation of a parabolic-index fiber in (4.16) is recalled and modified as

$$\left(\frac{2\pi\bar{a}}{\lambda}\right)^2 \left(n_1^2 - \eta^2\right) = 2\left(\frac{2\pi\bar{a}}{\lambda}\right)\left(n_1^2 - n_2^2\right)^{\frac{1}{2}}(2m + \ell + 1) \tag{4.38}$$

where $\bar{a}$ is the radius of the fiber. The taper may be locally approximated as a fiber of radius $\bar{a} = a - \alpha z$. Substituting for $\bar{a}$ in (4.38), we have

$$n_1^2 - \eta^2 = \frac{K}{a - \alpha z}, \quad K = \text{constant} \tag{4.39}$$

The constant $K = \left(\frac{\lambda}{\pi}\right)\left(n_1^2 - n_2^2\right)^{\frac{1}{2}}(2m + \ell + 1)$ may be determined in terms of η_0 by noting that $\eta(z = 0) = \eta_0$. Thus, z = 0 in (4.39) yields,

$$K = a\left(n_1^2 - \eta_0^2\right) \tag{4.40}$$

Combining (4.39) and (4.40), the result in (4.37) is obtained. Next, we calculate the term $n^2 - \eta^2$ in the R.H.S. of (4.36)

$$\begin{aligned} n^2 - \eta^2 &= n^2(r,z) - \eta^2(z) \\ &= n_1^2\left[1 - 2\Delta\left(\frac{r}{a - \alpha z}\right)^2\right] - \left[n_1^2 - \frac{a(n_1^2 - \eta_0^2)}{a - \alpha z}\right] \end{aligned}$$

$$= \frac{a(n_1^2 - \eta_0^2)}{a - \alpha z} - \left(2\Delta n_1^2\right)\frac{r^2}{(a - \alpha z)^2} \tag{4.41}$$

Introducing $\ell = \ell_0 k_0$ and using (4.41) in (4.36), we have

$$\eta_0^2\left(r\frac{dr}{dz}\right)^2 = a\left(n_1^2 - \eta_0^2\right)\frac{r^2}{a - \alpha z} - \left(2\Delta n_1^2\right)\frac{r^4}{(a - \alpha z)^2} - \frac{\ell^2}{k_0^2} \tag{4.42}$$

we further introduce R such that

$$R = \frac{r^2}{a(a - \alpha z)} \tag{4.43}$$

Using (4.43) in (4.42) and noting that

$$\eta_0^2\left(r\frac{dr}{dz}\right)^2 = \eta_0^2\left(\frac{1}{2}\frac{dr^2}{dz}\right)^2 = \eta_0^2\left[\frac{1}{2}\frac{d}{dz}\left(a(a - \alpha z)R\right)\right]^2$$

$$= \eta_0^2\left[\frac{a}{2}\left(-\alpha R + (a - \alpha z)\frac{dR}{dz}\right)\right]^2 \tag{4.44}$$

$$\approx \eta_0^2\left[\frac{a}{2}(a - \alpha z)\frac{dR}{dz}\right]^2 \quad ; \quad \alpha R << (a - \alpha z)\frac{dR}{dz}$$

we obtain

$$\frac{a}{2}(a - \alpha z)\frac{dR}{dz} = \frac{1}{\eta_0 k_0}\left(U_0^2 R - V^2 R^2 - \ell^2\right)^{\frac{1}{2}} \tag{4.45}$$

where $U_0^2 = (k_0 a)^2\left(n_1^2 - \eta_0^2\right)$ and $V^2 = (k_0 a)^2\left(n_1^2 - n_2^2\right) = (k_0 a)^2\left(2\Delta n_1^2\right)$

Rewriting (4.45) as

$$\frac{-\frac{\alpha}{a}dz}{\frac{a-\alpha z}{a}} = -\frac{\alpha\eta_0 k_0 a}{2}\frac{dR}{\left(U_0^2 R - V^2 R^2 - \ell^2\right)^{\frac{1}{2}}} \tag{4.46}$$

and integrating both sides, yields

$$\ln\left(\frac{a-\alpha z}{a}\right) = -\left(\frac{1}{2}\alpha\eta_0 k_0 a\right)\int \frac{dR}{\sqrt{-V^2R^2 + U_0^2 R - \ell^2}} + \text{constant} \tag{4.47}$$

But

$$\int \frac{dR}{\sqrt{-V^2R^2 + U_0^2 R - \ell^2}} = -\frac{1}{V}\sin^{-1}\left(\frac{-2V^2R + U_0^2}{\sqrt{U_0^4 - 4\ell^2V^2}}\right) \tag{4.48}$$

Substituting (4.48) in (4.47), we obtain

$$\underbrace{\frac{2V}{\alpha\eta_0 k_0 a}}_{\frac{2n_1\sqrt{2\Delta}}{\alpha\eta_0}}\ln\left(\frac{a-\alpha z}{a}\right) + \underbrace{\theta_0}_{\text{constant}} = \sin^{-1}\left(\frac{-2V^2R + U_0^2}{\sqrt{U_0^4 - 4\ell^2V^2}}\right)$$

or

$$\frac{-2V^2R + U_0^2}{\sqrt{U_0^4 - 4\ell^2V^2}} = \sin\left[\frac{2n_1\sqrt{2\Delta}}{\alpha\eta_0}\ln\left(\frac{a-\alpha z}{a}\right) + \theta_0\right] \tag{4.49}$$

Solving for R, yields

$$R = \frac{U_0^2}{2V^2} - \frac{\sqrt{U_0^4 - 4\ell^2V^2}}{2V^2}\sin\left[\frac{2n_1\sqrt{2\Delta}}{\alpha\eta_0}\ln\left(\frac{a-\alpha z}{a}\right) + \theta_0\right] \tag{4.50}$$

It may be noted that

$$\frac{U_0^2}{2V^2} = \frac{r_{01}^2 + r_{02}^2}{2a^2} \tag{4.51}$$

$$\frac{\sqrt{U_0^4 - 4\ell^2 V^2}}{2V^2} = \frac{r_{02}^2 - r_{01}^2}{2a^2} \tag{4.52}$$

where r_{01} and r_{02} are radii of caustics (on which turning points lie) for a parabolic-index fiber of radius a. That is,

$$r_{01} = \frac{a\sqrt{U_0^2 - \sqrt{U_0^4 - 4\ell^2 V^2}}}{\sqrt{2}V} \tag{4.53}$$

$$r_{02} = \frac{a\sqrt{U_0^2 + \sqrt{U_0^4 - 4\ell^2 V^2}}}{\sqrt{2}V} \tag{4.54}$$

Using (4.51) and (4.52) in (4.50), we obtain

$$R = \frac{1}{a^2}\left[\frac{r_{02}^2 + r_{01}^2}{2} - \frac{r_{02}^2 - r_{01}^2}{2}\sin\left[\frac{2n_1\sqrt{2\Delta}}{\alpha\eta_0}\ln\left(\frac{a-\alpha z}{a}\right) + \theta_0\right]\right] \tag{4.55}$$

Finally, putting (4.55) in (4.43), the expression for r as a function of z is obtained as

$$r = \sqrt{\frac{a-\alpha z}{a}}\left[\frac{r_{02}^2 + r_{01}^2}{2} - \frac{r_{02}^2 - r_{01}^2}{2}\sin\left(\frac{2n_1\sqrt{2\Delta}}{\alpha\eta_0}\ln\left(\frac{a-\alpha z}{a}\right) + \theta_0\right)\right]^{\frac{1}{2}} \tag{4.56}$$

θ_0 in (4.56) is a constant which may be determined using initial ray condition. This condition is chosen as $r = r_{01}$ at $z = 0$.

$$r_{01} = \left[\frac{r_{02}^2 + r_{01}^2}{2} - \frac{r_{02}^2 - r_{01}^2}{2}\sin\theta_0\right]^{\frac{1}{2}} \tag{4.57}$$

Clearly (4.57) is satisfied for $\theta_0 = \frac{\pi}{2}$. Putting this result in (4.106),we have

$$r = \sqrt{\frac{a-\alpha z}{a}}\left[\frac{r_{02}^2 + r_{01}^2}{2} - \frac{r_{02}^2 - r_{01}^2}{2}\cos\left(\frac{2n_1\sqrt{2\Delta}}{\alpha\eta_0}\ln\left(\frac{a-\alpha z}{a}\right)\right)\right]^{\frac{1}{2}} \tag{4.58}$$

A second equation for the ray trajectory is required. To find this equation we proceed as follows. From (4.27),

$$\frac{d\varphi}{ds} = \frac{d\varphi}{dz}\cdot\frac{dz}{ds} = \frac{d\varphi}{dz}\cdot\frac{\eta}{n} = \frac{\ell_0}{nr^2}$$

Thus,

$$\frac{d\varphi}{dz} = \frac{\ell_0}{\eta r^2} \tag{4.59}$$

However,

$$\frac{d\varphi}{dz} = \frac{d\varphi}{dr}\cdot\frac{dr}{dz}$$

hence,

$$\frac{d\varphi}{dr} = \frac{d\varphi/dz}{dr/dz} = \frac{\ell_0/\eta r^2}{\left(n^2 - \eta^2 - \frac{\ell_0^2}{r^2}\right)^{\frac{1}{2}}/\eta} = \frac{\ell_0 r}{r^2\left[r^2\left(n^2-\eta^2\right) - \ell_0^2\right]^{\frac{1}{2}}}$$

or

$$d\varphi = \frac{\frac{1}{2}\ell_0 d\left(r^2\right)}{r^2\left[r^2\left(n^2-\eta^2\right) - \ell_0^2\right]^{\frac{1}{2}}} \tag{4.60}$$

Using (4.41) and (4.43), we can write

$$\left[r^2\left(n^2-\eta^2\right) - \ell_0^2\right]^{\frac{1}{2}} = \left[a\left(n_1^2 - \eta_0^2\right)\frac{r^2}{a-\alpha z} - \left(2n_1^2\Delta\right)\frac{r^4}{\left(a-\alpha z\right)^2} - \frac{\ell^2}{k_0^2}\right]^{\frac{1}{2}}$$

$$= \frac{1}{k_0}\left[U_0^2 R - V^2 R^2 - \ell^2\right]^{\frac{1}{2}}$$

Then,

$$d\varphi = \frac{\frac{1}{2}\left(\frac{\ell}{k_0}\right) d\left[a(a-\alpha z)R\right]}{\left(\frac{a}{k_0}\right)(a-\alpha z)R\sqrt{-V^2R^2 + U_0^2R - \ell^2}} \tag{4.61}$$

But

$$d\left[a(a-\alpha z)R\right] = a\left[\underbrace{Rd(a-\alpha z)}_{-\alpha dz << dR} + (a-\alpha z)dR\right] \approx a(a-\alpha z)dR$$

Using this result in (4.61), yields

$$d\varphi = \frac{\frac{1}{2}\ell dR}{R\sqrt{-V^2R^2 + U_0^2R - \ell^2}} \tag{4.62}$$

Integrating both sides of (4.62), we have

$$\varphi = \frac{1}{2}\ell \int \frac{dR}{\sqrt{-V^2R^2 + U_0^2R - \ell^2}}$$

$$= \frac{1}{2}\ell\left[\frac{1}{\ell}\sin^{-1}\left(\frac{U_0^2R - 2\ell^2}{R\sqrt{U_0^4 - 4V^2\ell^2}}\right)\right] + \underbrace{\text{constant}}_{\frac{-\varphi_0}{2}}$$

$$\sin(2\varphi + \varphi_0) = \frac{U_0^2R - 2\ell^2}{R\sqrt{U_0^4 - 4V^2\ell^2}} \tag{4.63}$$

Substituting for R from (4.43),

$$\sin(2\varphi + \varphi_0) = \frac{U_0^2\left(\frac{r^2}{a(a-\alpha z)}\right) - 2\ell^2}{\sqrt{U_0^4 - 4V^2\ell^2}\left(\frac{r^2}{a(a-\alpha z)}\right)} \tag{4.64}$$

The constant φ_0 is determined from an initial ray condition. This condition is chosen such that at z = 0, $\varphi = \frac{\pi}{2}$. We recall that at z = 0, r = r_{01}. Thus,

$$\sin(\pi+\varphi_0) = -\sin\varphi_0 = \frac{U_0^2 r_{01}^2 - 2a^2\ell^2}{\sqrt{U_0^4 - 4V^2\ell^2}\,.\,r_{01}^2}$$

$$= \frac{U_0^2\left(U_0^2 - \sqrt{U_0^4 - 4\ell^2V^2}\right) - 4V^2\ell^2}{\sqrt{U_0^4 - 4V^2\ell^2}\left(U_0^2 - \sqrt{U_0^4 - 4\ell^2V^2}\right)}$$

$$= \frac{U_0^2\left(U_0^2 - \sqrt{U_0^4 - 4\ell^2V^2}\right) - 4V^2\ell^2}{-\left(U_0^2\left(U_0^2 - \sqrt{U_0^4 - 4\ell^2V^2}\right) - 4V^2\ell^2\right)} = -1$$

and $\varphi_0 = \frac{\pi}{2}$. Finally, the second equation for ray trajectory becomes,

$$\cos(2\varphi) = \frac{\dfrac{U_0^2 r^2}{a(a-\alpha z)} - 2\ell^2}{\sqrt{U_0^4 - 4V^2\ell^2}\,\dfrac{r^2}{a(a-\alpha z)}}$$

or

$$\cos(2\varphi) = \frac{U_0^2 r^2 - 2\ell^2 a(a-\alpha z)}{r^2\sqrt{U_0^4 - 4V^2\ell^2}} \tag{4.65}$$

In summary, equations (4.58) and (4.65) completely describe ray trajectories in graded-index fiber tapers. It is worth noting that when $\ell = 0$, r_{01} vanishes and (4.50) reduces to (4.32) which describes the trajectories for meridional rays.

4.3 Numerical Results

For a taper with specified parameters, ray trajectories are calculated using (4.32) for meridional rays and (4.58) and (4.65) for skew rays. The parameters of the taper used to obtain numerical results are : a=100 μm, b=25 μm, L=1cm, n_1=1.5, n_2= 1.48. In

calculating ray trajectories, the characteristic equation (4.16) together with (4.53) and (4.54) are used to determine U_0, η_0, r_{01} and r_{02} for the specified parameters and wavelength of operation. For this example λ = 1.3 μm has been chosen. Figure 4.3 illustrates the three-dimensional view of a meridional ray for an LP_{01} mode corresponding to the LP_{01} mode in a uniform (untapered) fiber with a core radius equal to the larger end radius of the taper and the same index profile as the taper. The behavior of this ray, and meridional rays in general, is similar to the rays in planar tapered waveguides, with the implication that two-dimensional planar tapers may serve as simplified models for three dimensional fiber tapers when meridional rays are considered. As an example of a skew ray, in the same fiber taper and for the same wavelength of operation, Figure 4.4a shows the ray trajectory corresponding to the LP_{13} mode of the untapered fiber. The two-dimensional views of this ray in the xz and xy planes are shown in Figures 4.4b and 4.4c, respectively. These figures clearly illustrate the gradual concentration of ray power towards the smaller end of the taper. A quantitative analysis of focusing capability of tapers will be presented in the next chapter.

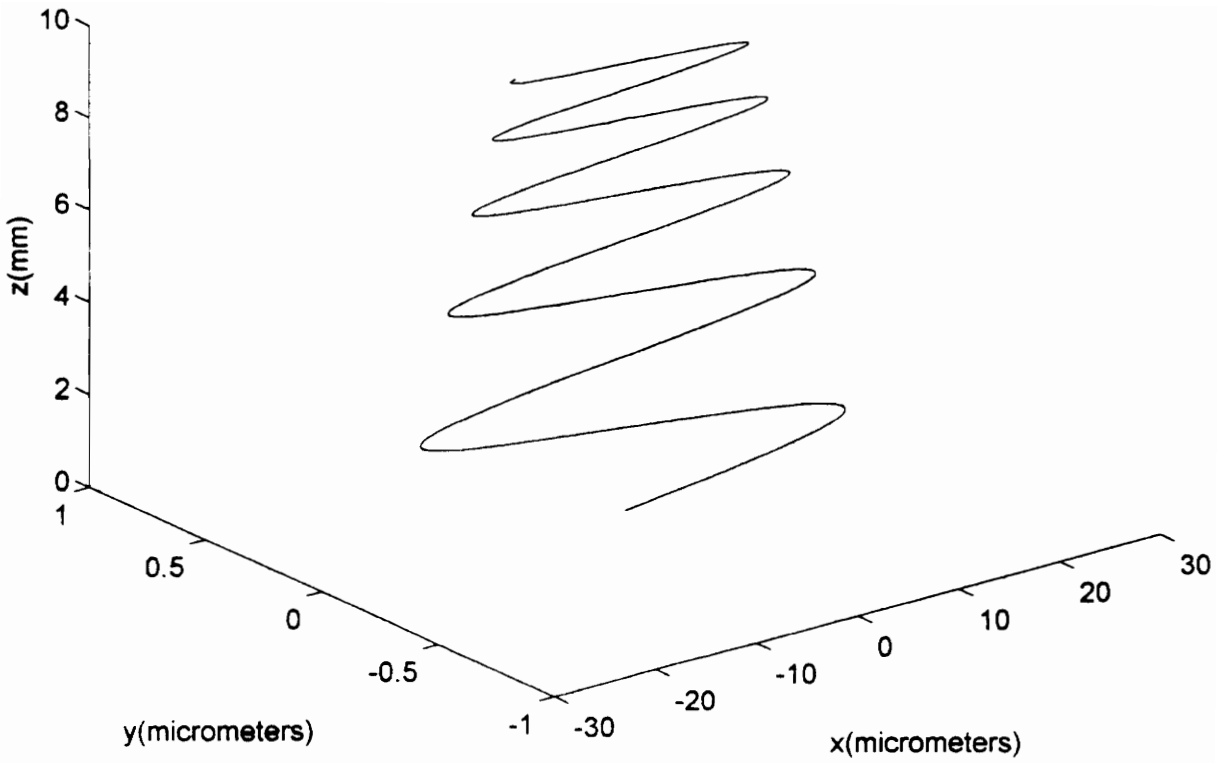

Figure 4.3 Three dimensional trajectory of a meridional ray corresponding to LP_{01} mode in a linearly tapered parabolic-index fiber with a=100 μm, b=25 μm, L =1 cm, n_1=1.5, and n_2 = 1.48.

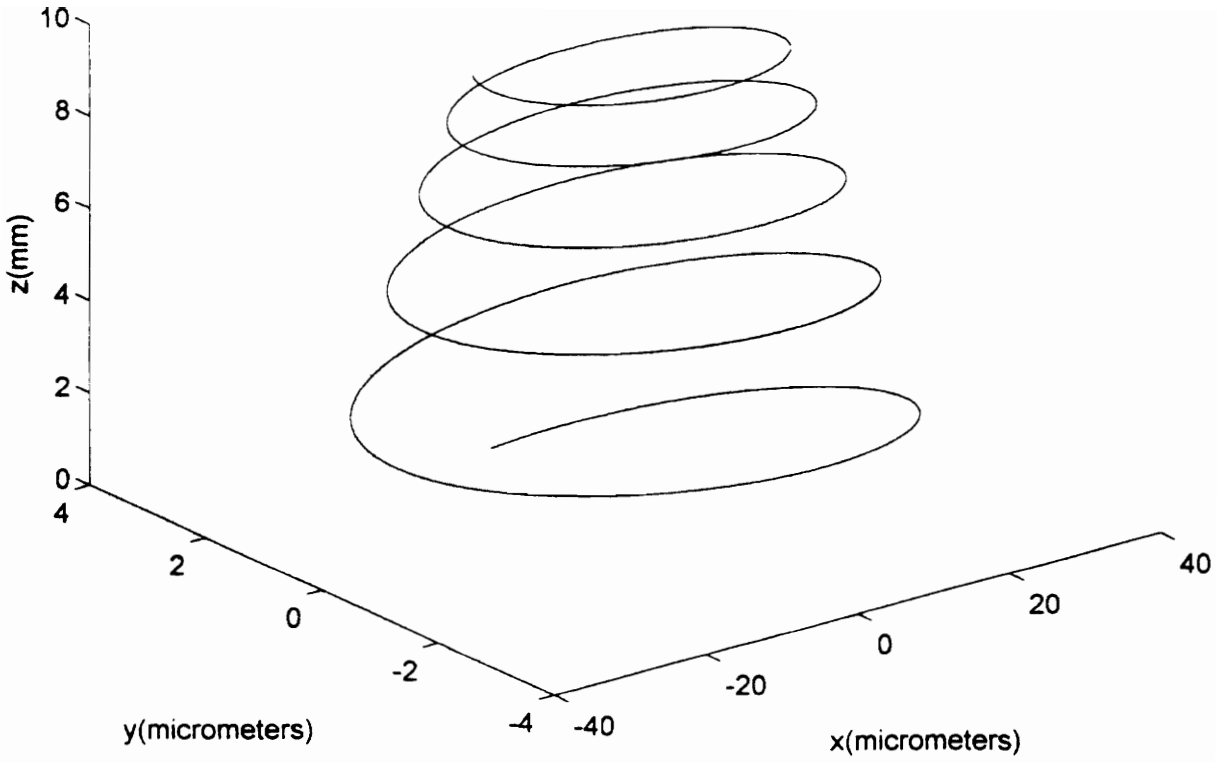

Figure 4.4a Three dimensional ray trajectory of a skew ray corresponding to LP_{13} mode in a linearly tapered parabolic-index fiber with a=100 μm, b=25 μm, L =1 cm, n_1=1.5, and n_2 = 1.48.

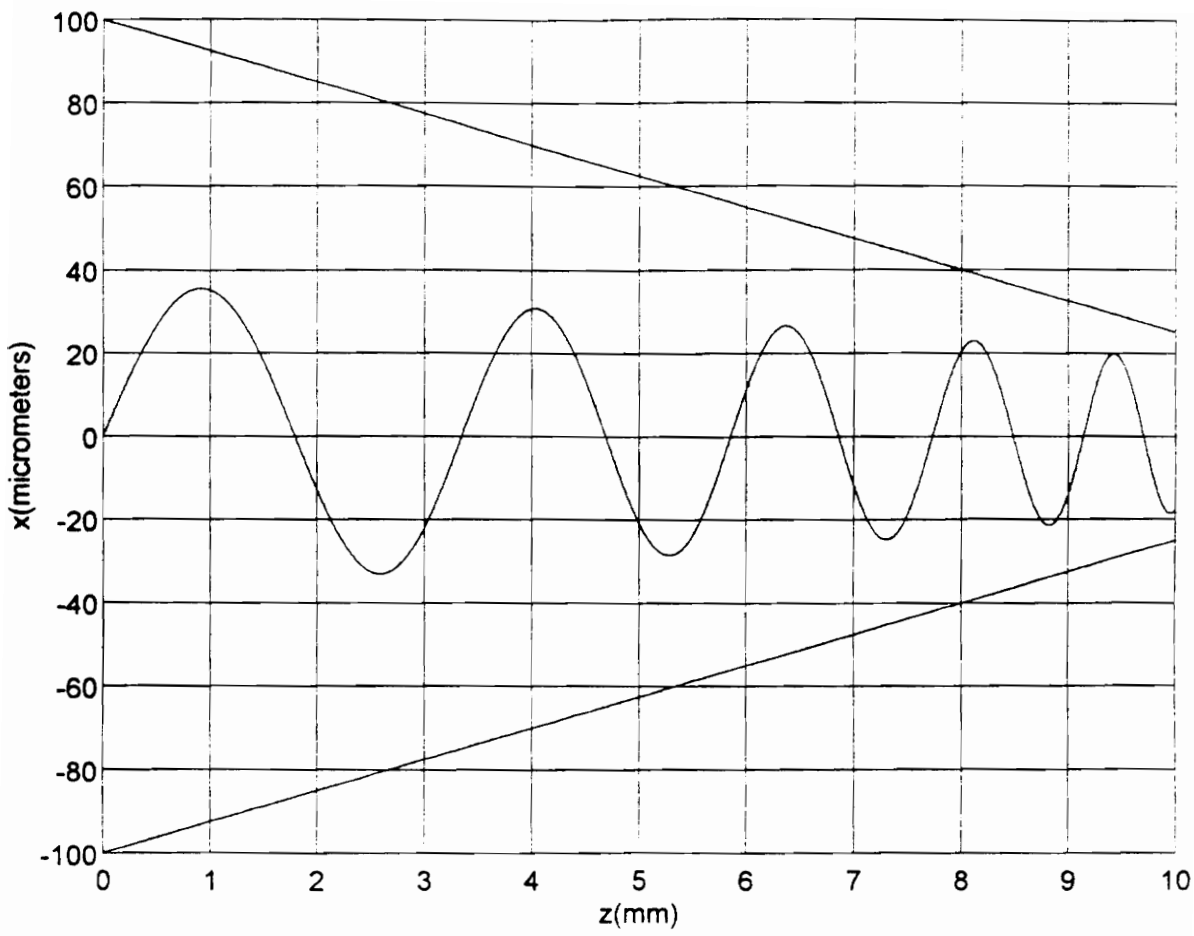

Figure 4.4b Projection of the ray in Figure 4.4a onto the xz plane.

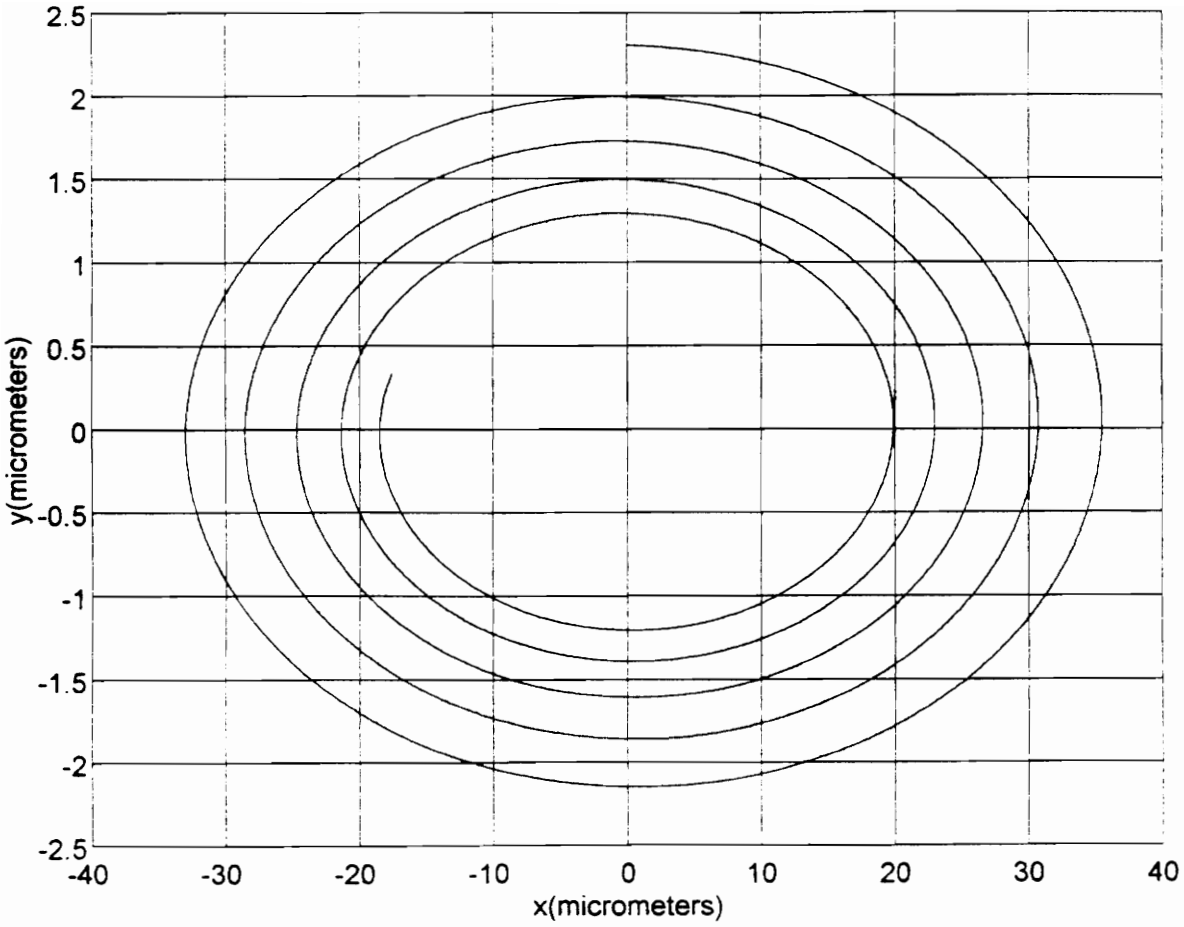

Figure 4.4c Projection of the ray in Figure 4.4a onto the xy plane.

5. Coupling Efficiency and Radiation Loss

Important applications of graded-index tapers discussed in Chapters 3 and 4 include their use to couple power from light sources into planar or fiber lightguides and as transition elements between two guides of different core sizes. Coupling efficiencies when tapers are used to couple power from collimated beam and Lambertian light sources into lightguides are calculated. Also, radiation loss of tapers when used to connect two multimode waveguides with different core areas is determined. Numerical results for coupling efficiency, radiation loss and improvement in coupling efficiency are presented.

5.1 Coupling Efficiency

5.1.1 Tapered Planar Waveguides

For collimated-beam illumination, substituting $\alpha_0 = 0$ in (3.50), the condition for rays to be bound to the core of the taper is determined as

$$|x_1| \le \sqrt{ab}\left(1-\frac{\alpha^2}{8\Delta}\right) \approx \sqrt{ab} \tag{5.1}$$

Let us consider a light source of thickness 2d attached to the larger end of a parabolic-index tapered waveguide with parameters as in Figure 3.2. The smaller end of the taper is assumed to be connected to a waveguide of thickness $2b$. We denote the source power, the bound rays power and the power coupled into the waveguide of thickness $2b$ directly from the source as P_s, P_1, and P_2, respectively. The coupling efficiency for the taper(η) and the improvement in coupling efficiency(I) for the waveguide of the thickness $2b$ are defined as

$$\eta = \frac{P_1}{P_s} \tag{5.2}$$

$$I = \frac{P_1}{P_2} \tag{5.3}$$

When d is less than or equal to b, $P_s = P_1 = P_2 = 2p_0 d$ are calculated. If d is between b and $\sqrt{ab}$, $P_s = P_1 = 2p_0 d$, and $P_2 = 2p_0 b$ are obtained. For $d > \sqrt{ab}$, we have $P_s = 2p_0 d$, $P_1 = 2p_0\sqrt{ab}$, and $P_2 = 2p_0 b$. Using these results in (5.2) and (5.3), the coupling efficiency η and improvement in coupling efficiency I are determined as

$$\eta = \begin{cases} \dfrac{\sqrt{ab}}{d} & , \ d > \sqrt{ab} \\ 1 & , \ d \le \sqrt{ab} \end{cases} \tag{5.4}$$

$$I = \begin{cases} \sqrt{\dfrac{a}{b}} & ,d > \sqrt{ab} \\ \dfrac{d}{b} & ,b < d \le \sqrt{ab} \\ 1 & ,d \le b \end{cases} \tag{5.5}$$

For the taper of Figure 4.3 with $a = 100$ μm and $b = 25$ μm, from (5.4) a coupling efficiency of 100 % can be obtained if the taper is used to couple a collimated beam source with a width $(2d)$ equal to or less than 100 μm to a waveguide of thickness $2b$. Also, it is clearly seen from (5.5) that up to two times more power can be launched into the waveguide compared to direct launching of the beam into it.

For a Lambertian source, which emits light over a broad beam, the radiation pattern is approximated as $I = I_0 \cos\theta$, where I_0 is the axial intensity and θ is the angle of emission. Then, P_1 is calculated as

$$P_1 = 2p_0 \int_0^c \int_{\theta_1}^{\theta_2} \cos\theta d\theta dx = 2p_0 \int_0^c (\sin\theta_2 - \sin\theta_1) dx \tag{5.6}$$

where $c = \sqrt{ab}$ if $d > \sqrt{ab}$ and $c = d$ if $d \le \sqrt{ab}$, $\theta_1 = \tan^{-1}(\alpha_{01})$, and $\theta_2 = \tan^{-1}(\alpha_{02})$. For $\Delta << 1$ and $\alpha << 1$, both α_{01} and α_{02} are much smaller than unity, then using the approximation $\sin\theta_2 - \sin\theta_1 \approx \theta_2 - \theta_1 \approx \alpha_{02} - \alpha_{01} = 2\sqrt{2\Delta T}$ where T is defined in (3.51), P_1 in (5.6) becomes

$$P_1 = 4p_0 n_1 \sqrt{2\Delta} \int_0^c \sqrt{\frac{b}{a} - \left(\frac{x}{a}\right)^2} dx \tag{5.7a}$$

$$= 2p_0 n_1 \sqrt{2\Delta}\sqrt{\frac{b}{a}}\left[c\sqrt{1-\frac{c^2}{ab}} + \sqrt{ab}\sin^{-1}\left(\frac{c}{\sqrt{ab}}\right)\right] \quad (5.7b)$$

And the source power P_s is calculated as

$$P_s = 2p_0\int_0^d\int_{-\frac{\pi}{2}}^{\frac{\pi}{2}}\cos\theta d\theta dx = 2p_0\pi d \quad (5.8)$$

In a similar manner, the power P_2 is obtained as

$$P_2 = 2p_0\int_0^h\int_{\theta_1}^{\theta_2}\cos\theta d\theta dx = 2p_0\int_0^h 2NA(x)dx$$

$$= 4p_0 n_1\sqrt{2\Delta}\int_0^h\sqrt{1-\left(\frac{x}{b}\right)^2}dx \quad (5.9a)$$

$$= 2p_0 n_1\sqrt{2\Delta}\left[h\sqrt{1-\left(\frac{h}{b}\right)^2} + b\sin^{-1}\left(\frac{h}{b}\right)\right] \quad (5.9b)$$

where $h = b$ if $d > b$ and $h = d$ if $d \le b$. With the help of (5.6)-(5.9), the coupling efficiency η and improvement in coupling efficiency I are readily calculated. Considering the case when $d \ge \sqrt{ab} > b$, $P_1 = P_2 = p_0\pi n_1 b\sqrt{2\Delta}$ are obtain from (5.7b) and (5.9b). Then, $I = 1$, indicating that the taper cannot improve the coupling efficiency when the light source is Lambertian type such as surface emitting LED.

5.1.2 Tapered Fibers

Compared to the case of planar waveguides in which only meridional rays exist, evaluation of coupling efficiency for tapered fibers becomes more complicated because

the problem is three dimensional and both meridional and skew rays must be accounted for. However, for a collimated beam, from (4.59) and (4.60), we can easily show that parallel rays getting into the taper are meridional rays. For meridional rays to be bound to the core of the taper, the following condition should be satisfied

$$|r_{01}| \le \sqrt{ab}\left(1-\frac{\alpha^2}{8\Delta}\right) \approx \sqrt{ab} \tag{5.10}$$

Let us consider a light source of circular cross section with radius d attached to the larger end of a parabolic-index tapered fiber with parameters as in Figure 4.2. The smaller end of the taper is assumed to be of the radius b. The source power, the bound rays power, and the power coupled into a fiber of radius b directly from the source can now be calculated as $P_s = p_0\pi d^2$, $P_1 = p_0\pi c^2$, where $c = \sqrt{ab}$ if $d > \sqrt{ab}$ and $c = d$ if $d \le \sqrt{ab}$ and $P_2 = p_0\pi h^2$ where $h = b$ if $d > b$ and $h = d$ if $d \le b$. Then, the coupling efficiency (η) and the improvement in coupling efficiency (I), defined in (5.2) and (5.3), are summarized as

$$\eta = \begin{cases} \dfrac{ab}{d^2} & , \ d > \sqrt{ab} \\ 1 & , \ d \le \sqrt{ab} \end{cases} \tag{5.11}$$

$$I = \begin{cases} \dfrac{a}{b} & , d > \sqrt{ab} \\ \dfrac{d^2}{b^2} & , b < d \le \sqrt{ab} \\ 1 & , d \le b \end{cases} \tag{5.12}$$

5.2 Radiation Loss

Let us consider two parabolic-index waveguides, referred to as waveguides 1 and 2, with core thicknesses $2a$ and $2b$, respectively, connected by a taper of length L as shown in Figure 5.1. Both waveguides are assumed to have the same cladding index (n_2) and the same Δ parameter. Clearly P_1 is the input power to the taper too and the power coupled into waveguide 2 from the taper is assumed to be P_2. Then the radiation loss of the taper is defined as

$$L_r(dB) = 10\log_{10}\left(\frac{P_1}{P_2}\right) \tag{5.13}$$

Assuming that the area of the source is equal to or larger than the core area of waveguide 1, that is d $\geq a$, the power $P_1 = p_0 \pi n_1 a\sqrt{2a}$ is determined from (5.9b) by substituting both h in the upper limit of the integral and b in the integrand with a. The power $P_2 = p_0 \pi n_1 b\sqrt{2\Delta}$ is also obtained from (5.7b) with $c = \sqrt{ab}$. Then, the radiation loss is given as

$$L_r(dB) = 10\log_{10}\left(\frac{a}{b}\right) \tag{5.14}$$

If waveguides 1 and 2 are butt coupled such that their axes are perfectly aligned and reflection losses due to mismatch of the core indices are neglected and further a uniform distribution of power among the modes of waveguide 1 is assumed, it can be shown that the splice loss between them will be the same as the radiation loss of the taper given in

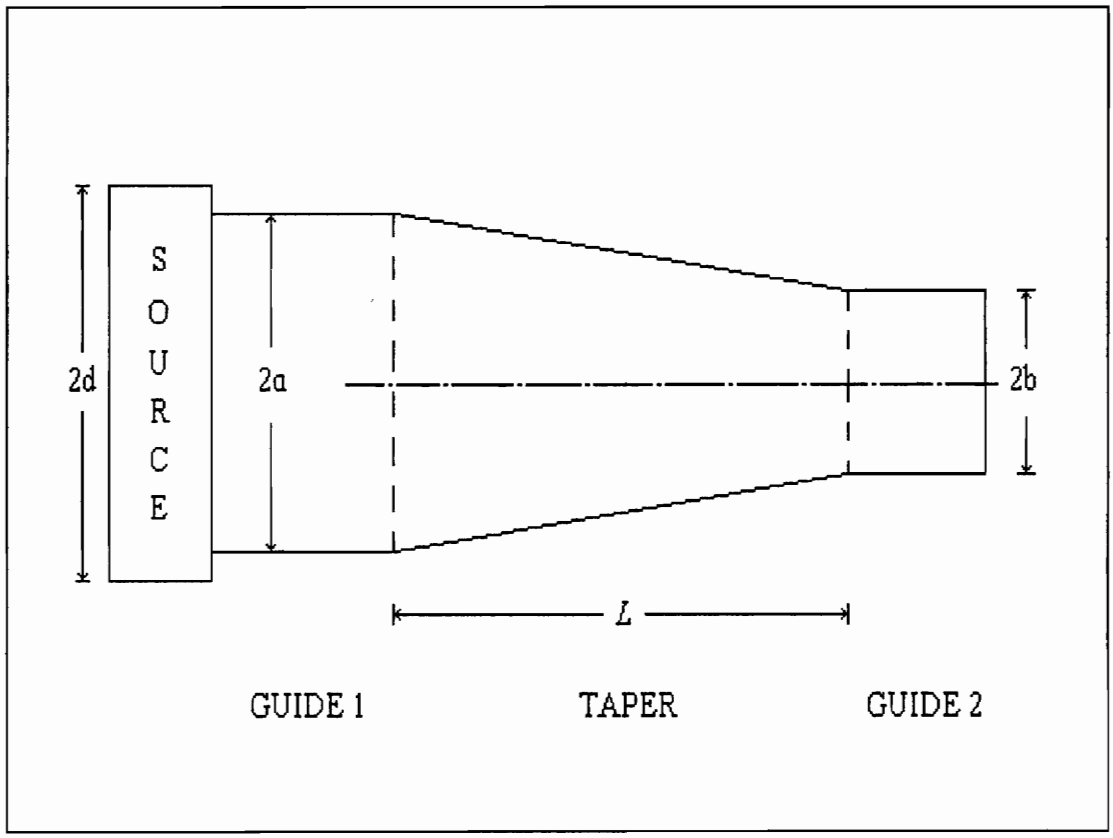

Figure 5.1 Parabolic-index taper connecting two waveguides with different core areas. A Lambertian light source excites the waveguide with larger core area.

(5.14). To see this, the splice loss is calculated as follows: This loss is estimated as the ratio of the common mode volume to the number of modes in waveguide 1 [28]. The number of modes is obtained as $M = \left(\frac{4\pi t}{\lambda}\right) n_1 \sqrt{2\Delta}$, where λ is the wavelength of the light, by using the transverse resonance condition of bound rays in a parabolic-index slab waveguide of thickness $2t$ [30]. To find the number of modes in waveguide 1 and the common mode volume, we need to replace t in the expression for M with a and b, respectively and then the splice loss in dB is calculated as $L_s = 10\log_{10}\left(\frac{a}{b}\right)$ which is equal to the radiation loss in (5.14).

The radiation loss of a fiber taper excited by a Lambertian source is also the same as splice loss resulting from direct coupling of two fibers of radii a and b. Assuming equal distribution of power among the modes, this loss is estimated as

$$L_r(dB) = 10\log_{10}\left(\frac{a^2}{b^2}\right)$$

$$= 20\log_{10}\left(\frac{a}{b}\right) \qquad (5.15)$$

5.3 Beam Concentrator

As we have seen, tapers can gradually concentrate light rays along their axis. To make a light beam concentrator for parallel rays; however, with specific values of taper parameters (a, α, n_1 and n_2), the length of the taper must be chosen such that rays at

the output of the taper become parallel. To find the appropriate length, since $\alpha_0 = 0$ we substitute $\eta = n_1$ in (4.32) and obtain

$$r = r_0 \sqrt{\frac{a - \alpha z}{a}} \sin\left[\sqrt{\frac{2\Delta}{\alpha^2} - \frac{1}{4}} \ln\left(\frac{a - \alpha z}{a}\right) + \theta_0\right] \tag{5.16}$$

Since parallel rays should have their slope equal to zero, we differentiate (5.16) and set it equal to zero. Then

$$\tan\left[\frac{1}{2}\sqrt{-1 + \frac{8\Delta}{\alpha^2}} \ln\left(\frac{a - \alpha z}{a}\right)\right]\left[2 - \frac{8\Delta}{\alpha^2}\right] + 2\sqrt{\frac{8\Delta}{\alpha^2} - 1} = 0 \tag{5.17}$$

Assuming that $\frac{\alpha^2}{8\Delta} << 1$, the solution of (5.17) for z is obtained as

$$z = L_0 = \frac{a}{\alpha}\left[1 - e^{\frac{2\alpha}{\sqrt{8\Delta}}\left[\tan^{-1}\left(\frac{2\alpha}{\sqrt{8\Delta}}\right) - n\pi\right]}\right], \quad n = 1,2,3,\ldots \tag{5.18}$$

A collimated beam of parallel rays entering a taper with length L_0 leaves the taper as a concentrated beam. Figure 5.2 illustrates ray trajectories of parallel rays entering into a taper with a=100 μm, $\alpha = 6.33 \times 10^{-3}$, $\Delta = \frac{1.5^2 - 1.48^2}{2 \times 1.5^2} = 0.013244$ and L=11.6685 mm. In this example the radius of the beam is reduced by a factor of 2.

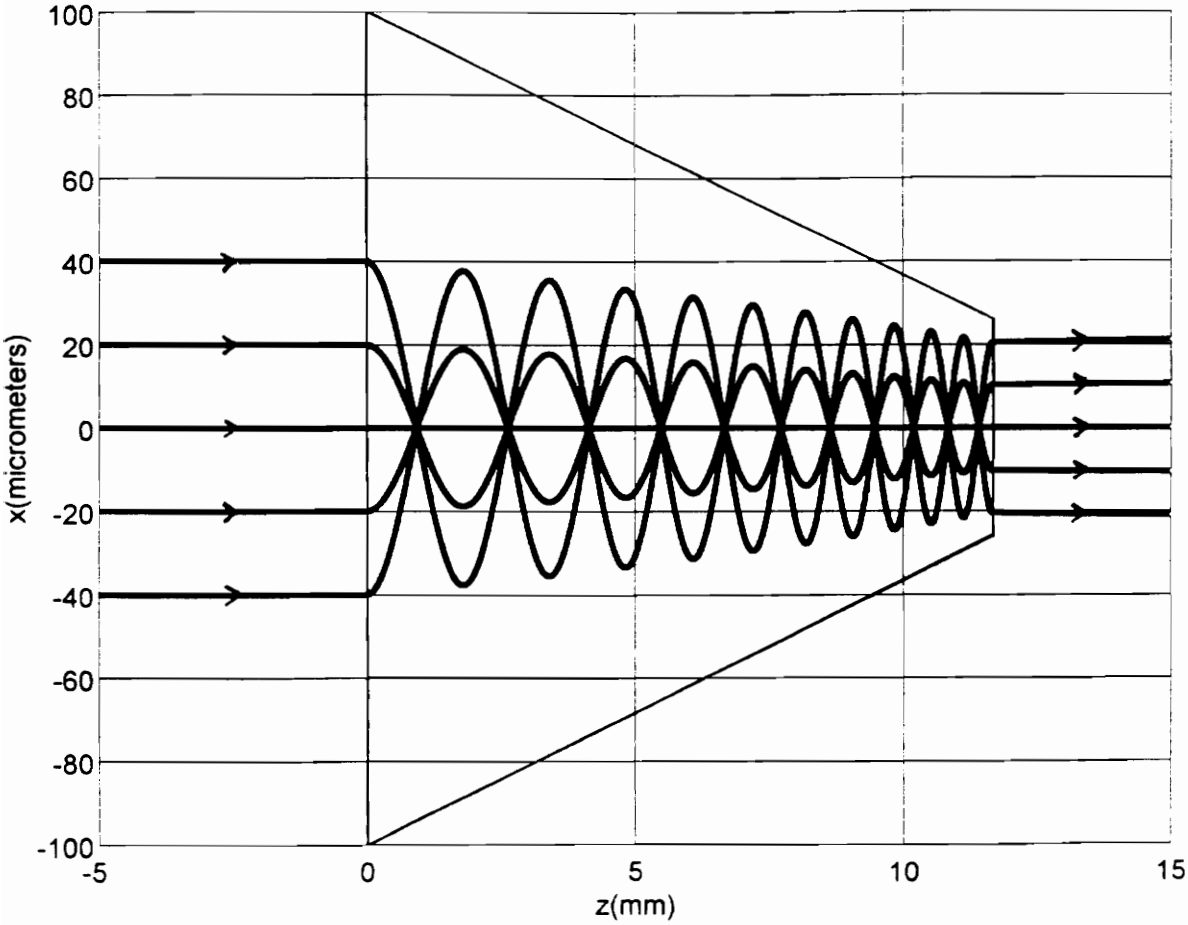

Figure 5.2 Ray trajectories of parallel rays entering into the taper with a =100 μm, $\alpha = 6.33 \times 10^{-3}$, $\Delta = 0.013244$, and L =11.6685 mm.

6. Conclusions and Suggestions for Further Research

This thesis has addressed light propagation in multimode parabolic-index tapers. Two types of tapers have been examined, including planar waveguide and optical fiber tapers. A ray-optic approach has been used to study the transmission properties of tapers. Analytical solutions of ray equations have been obtained for tapers with small slope and small difference between the refractive indices of core and cladding. These conditions (small slope and small index difference) are readily satisfied for tapers made of commercially available graded-index fibers or preforms. Ray trajectories for both meridional and skew rays have been obtained. These trajectories clearly illustrate the light focusing capability of graded-index tapers.

Graded-index tapers may find important applications for coupling light sources to planar waveguides and optical fibers as well as for splicing two waveguides or fibers with different core sizes. Coupling efficiencies for collimated beam and Lambertian light

sources have been calculated. The tapers provide significant improvement in power coupling of focused beam sources. In addition, they can improve alignment tolerances of source to waveguide or fiber coupling. A novel application of taper as optical power concentrator has been introduced.

The work presented in this thesis has been limited to linearly tapered planar waveguides and optical fibers. Nonlinear tapers, in particular those with exponential taper profile, are worth further investigations. Optimization of taper profile in order to achieve maximum coupling efficiency or minimum radiation loss is also of practical significance and needs further investigation. The optimization can be extended to the index profile of the taper, too. Comparison of power concentrating capabilities of tapers with different index profiles, including step-index, parabolic index, triangular index and α - power index profiles, needs to be examined.

REFERENCES

1. R. Zengerle, O. Leminger, W. Weiershausen, K. Faltin and B. Hübner, "Laterally tapered InP-InGaAsP waveguides for low-loss chip-to-fiber butt coupling: A comparison of different configurations", IEEE Photonics Technol. Lett., vol. 7, no. 5, pp. 532-534, 1995.

2. N. Yoshimoto, K. Kawano, H. Takeuchi, S. Kondo and Y. Noguchi, "Highly efficient coupling semiconductor spot-size converter with an InP/InAlAs multi-quantum-well core", Applied Optics, vol. 34, no. 6, pp.1007-1014, 1995.

3. D. Intani, T. Baba and K. Iga, "Planar microlens relay optics utilizing lateral focusing", Applied Optics, vol. 31, no. 25, pp. 5255-5258, 1992.

4. D. Intani, T. Baba and K. Iga, "Simple optical wavelength-division multiplexer component that uses the lateral focusing scheme of a planar microlens", Applied Optics, vol. 33, no. 16, pp. 3405-3408, 1994.

5. Y. Uematsu and T. Ozeki, "Efficient power coupling between an MH LED and a taper-ended multimode fiber", IEEE J. Quantum Electron., vol. QE-15,no. 2, pp. 86-92, 1979.

6. H. Kuwahara and H. Furuta, "Efficient light coupling from semiconductor lasers into tapered hemispherical-end fibers", Proceedings of the IEEE, vol. 67, no. 10, pp. 1456-1457, 1979.

7. H. Kuwahara, M. Sasaki and N. Tokoyo, "Efficient coupling from semiconductor lasers into single-mode fibers with tapered hemispherical ends", Applied Optics, vol. 19, no. 15, pp. 2578-2583, 1980.

8. G. D. Khoe, J. Poulissen and H. M. de Vrieze, "Efficient coupling of laser diodes to tapered monomode fibers with high-index end", Electronics Letters, vol. 19, no. 6, pp. 205-207, 1983.

9. H. M. Presby, N. Amitay, R. Scotti and A. F. Benner, "Laser-to-fiber coupling via optical fiber up-tapers", J. lightwave Technol., vol. 7, no. 2, pp. 274-278, 1989.

10. T. Ozeki and B. S. Kawasaki, "Optical directional coupler using tapered sections in multimode fibers", Applied Physics Letters, vol. 28, no. 9, pp. 528-529, 1976.

11. T. Ozeki, T. Ito and T. Tamura, "Tapered section of multimode cladded fibers as mode filters and mode analyzers", Applied Physics Letters, vol. 26, no. 7, pp. 386-

388, 1975.

12. K. A. Murphy, B. R. Fogg and A. M. Vengsarkar, "Spatially weighted vibration sensors using tapered two-mode optical fibers", J. lightwave Techno., vol. 10, no. 11, pp. 1680-1687,1992.

13. C. D. Singh and B. D.Gupta, "Detection of gases with porous-clad tapered fibers", Applied Optics, vol. 34, no. 6, pp. 1019-1023, 1995.

14. Z. M. Hale and F. P. Payne, "Fluorescent sensors based on tapered single-mode optical fibres", Sensors and Actuators B, vol 17, pp. 233-240, 1994.

15. M. Dakss, L. Kuhn, P. Heidrich and B. Scott, "Grating coupler for efficient excitation of optical guided waves in thin films," Appl. Phys. Lett., vol. 16, pp. 523-527, 1970.

16. K. Ogawa, W. Chang, B. Sopori and F. Rosenbaum, " A theoretical analysis of etched grating couplers for integrated optics," IEEE J. Quantum Electron., vol. QE-9, pp. 29-42, 1973.

17. T. A. Strasser, W. Y. Hsu and M. C. Gupta, "Grating coupler acceptance design utilizing a tapered waveguide structure", Applied Optics, vol. 32, no. 30, pp. 6006-6017, 1993.

18. J. C. Brazas, L. L., and A. L. McKeon, "High-efficiency input coupling into optical waveguides using gratings with double-surface corrugation", Applied Optics, vol. 34,

no. 4, pp. 604-609, 1995.

19. G.N. Lawrence and S.-H. Hwang, "Beam propagation in gradient refractive-index media", Applied Optics, vol. 31, no. 25, pp. 5201-5210, 1992.

20. J. Puchalski, "Numerical determination of ray tracing: a new method", Applied Optics, vol. 31, no. 31, pp. 6789-6799, 1992.

21. T. Touam and F. Yergeau, "Analytical solution for a linearly graded-index-profile planar waveguide", Applied Optics, vol. 32, no. 3, pp. 309-312, 1993.

22. B. Szafraniec and B. E. Briley, "Geometric optics analysis of modal propagation in graded-index cylindrical fiber", Applied Optics, vol. 29, no. 12, pp.1772-1779, 1990.

23. J. Linares and C. Gomez-Reino, "Focal curves generated by one-dimensional GRIN tapers", Opt. Lett., vol. 15, pp. 1258-1260, 1990.

24. R. M. Gonzalez, J. Linares and C. Gomez-Reino, "Three-dimensional focal curves generated by one-dimensional gradient-index tapers", Applied Optics, vol. 31, no. 25, pp. 5171-5177, 1992.

25. A. Cutolo, L. Carlomusto, F. Reale and I. Rendina, "Tapered and inhomogeneous dielectric light concentrators", Applied Optics, vol. 29, no. 9, pp.1353-1364, 1990.

26. L. W. Casperson, "Beam propagation in tapered quadratic-index waveguides:

Analytical solutions", J. lightwave techno., vol. LT-3, no. 2, pp. 264-272, 1985.

27. A. A. Tovar and L. W. Casperson, "Beam propagation in parabolically tapered graded-index waveguides", Applied Optics, vol. 33, no. 33, pp. 7733-7739, 1994.

28. G. Keiser, Optical Fiber Communications, McGraw-Hill, Inc., New York, 1991.

29. A. Safaai-Jazi, Lecture Notes on optical waveguides, Department of Electrical Engineering, Virginia Polytechnic Institute and State University, 1988.

30. M. J. Adams, An Introduction to Optical Waveguides, John Wiley and Sons, Chichester, ch. 3, 1981.

Appendix A. Program for calculating ray trajectories in tapered planar waveguides

The MATLAB source code was used to calculate both exact and approximate solutions of ray trajectories in tapered planar waveguides presented in section 3.2.3. The following input data are required to execute the program.

- **Number of sections** - Sampling points of the calculated results. For larger number of points, the ray trajectories are smoother and more accurate.

- **A** - Thickness of the core at the beginning of the taper.

- **B** - Thickness of the core at the end of the taper.

- **L** - The Length of the taper.

• **N1** - The refractive index on the axis of the taper.

• **N2** - The refractive index of the cladding of the taper.

• **ALPHA_ZERO** - the slope of the ray at the beginning of the taper.

Below is a listing of the program.

```
% % % % % % % % % % % % % % % % % % % %
%                                       %
%                                       %
%    SUBROUTINE  FOR  INPUT DATA        %
%                                       %
%                                       %
% % % % % % % % % % % % % % % % % % % %

 no_section = input('How many sections? ');
 a_size = input('input the thickness A for the beginning end (m) > ');
 b_size = input('input the thickness B for the ending end (m) >  ');
 l_size = input('input Length of the fiber to calculate alpha (m) >  ');
 n1 = input(' input inner index (N1) >  ');
 n2 = input(' input outer index (N2) >  ');
alpha_zero = (‘input alpha at the beginning of the taper >‘);
 beta = n1/sqrt(1+alpha_zero^2);
 end

% % % % % % % % % % % % % % % % % % % %
%                                       %
%                                       %
%    SUBROUTINE FOR CALCULATING         %
%      THE APPROXIMATE SOLUTION         %
%                                       %
%                                       %
% % % % % % % % % % % % % % % % % % % %

    step_size = l_size/no_section;
    n = no_section +1;
    z = 0;
    q2 = 0;
```

```
    min = 1e-10;
    l0 = sqrt((n1^2)/(beta^2)-1);
   alpha = (a_size-b_size)/l_size;
   delta = (n1^2-n2^2)/(2*n1^2);

   x0=-1*sqrt((l0*a_size/alpha)^2/(2*delta*n1^2/(alpha*beta)^2 - 1/4));
  phi0 = 0;

  for p = 1:n

    if q2 == 0
        ai=(a_size-alpha*z)/a_size;
       c1 = sqrt((2*delta*n1^2)/((beta^2)*(alpha^2))-(1/4));
       x(p) = x0*sqrt(ai)*sin(c1*log(ai)+phi0);
    else
       x(p) = slope*(z-za) + xa;
    end
% end if and else q2 == 0

      check = a_size -alpha*z ;

      if abs(x(p)) > check
        q2 = q2 +1 ;
         if q2 == 1
        disp(' >>>>>>> Leaking !!! >>>>>>>');
        pause;
            xa = x(p);
           za = z;
           xb = x(p-1);
           slope = (xa-xb)/step_size;
         end
      end

       az(p) = z*1e3;
         ax(p) = x(p)*1e6;

      if abs(ax(p)) < min
        ax(p) = 0;
      end
    z = z + step_size;
end
% end for p = 1:n
```

```
% % % % % % % % % % % % % % % % % % % %
%                                       %
%                                       %
%    SUBROUTINE FOR CALCULATING         %
%    THE EXACT SOLUTION                 %
%                                       %
%                                       %
% % % % % % % % % % % % % % % % % % % % %

    ci = 1;
    c4=ci+1;
    cp =1;
    step_size = l_size/(no_section*ci);
    z = 0;
    q2 = 0;
    min = 1e-10;
   alpha = (a_size-b_size)/l_size;
   delta = (n1^2-n2^2)/(2*n1^2);
   xi(1) = 0;
   li(1) = sqrt((n1^2/beta^2)-1);

   for t = 1:no_section
    ai(t) =a_size-alpha*(t-1)*(l_size/no_section);
    zi(t) =(t-1)*(l_size/no_section);
    index=n1*(1-(delta*xi(t)^2)/(a_size-alpha*zi(t))^2);
    betai(t) = index/sqrt(1+li(t)^2);
    st1 = n1*sqrt(2*delta)/(betai(t)*ai(t));
    if li(t) == 0
       phi(t) = asin(1);
       x0(t) = xi(t);
    else
       phi(t) = atan(xi(t)*st1/li(t));
       x0(t) = li(t)/(cos(phi(t))*st1);
    end
   for tp = 1:c4
     if q2==0
        x=x0(t)*sin(st1*(z-zi(t))+phi(t));
     else
       x = slope*(z-za)+xa;
     end
     check = a_size-alpha*z;
       if abs(x) > check
        q2 = q2+1;
```

```
          if q2==1
         disp(' >>>>>>> Leaking !!! >>>>>>>');
         pause;
            xa = x;
            za = z;
            xb = x0(t)*sin(st1*((z-step_size)-zi(t))+phi(t));
            slope=(xa-xb)/step_size;
           end
       end

       if tp == c4 & t<no_section
          xi(t+1) =x;
          angle=x0(t)*st1*cos((st1*l_size/no_section)+phi(t));
          li(t+1)=angle;
       else
        ez(cp) = z*1e3;
           ex(cp) = x*1e6;
          if abs(ex(cp)) < min
            ex(cp) = 0;
          end
         z = z + step_size;
          cp =cp+1;
       end
end
% end for tp = 1:c4
end
% end for t = 1:no_section

% % % % % % % % % % % % % % % % % % % % %
%                                       %
%                                       %
%    SUBROUTINE FOR DISPLAYING          %
%    THE GRAPH                          %
%                                       %
%                                       %
% % % % % % % % % % % % % % % % % % % % %

    up_step = alpha*l_size/100 ;
    dw_step = up_step  ;
    fz_step = l_size/100 ;
    fz = 0;
    for p = 1:101
       up(p) = 1e6*(a_size-(p-1)*up_step)   ;
```

```
        dw(p) = -1e6*(a_size-(p-1)*dw_step)   ;
        sz(p) = 1e3*(fz + (p-1)*fz_step)      ;
      end
plot(az,ax,'-',sz,up,'-',sz,dw,'-',ez,ex,'.');
 title('Approximated and Exact ray trajectories in Tapered waveguide');
    xlabel('z(mm)');
    ylabel('x(micrometers)');
  grid;
    print -dwin;
    pause;
    close;
    end
```

Vita

Voravut Suppanitchakij was born to Paisal and Naiyana Suppanitchakij on November 20, 1971 in Bangkok, Thailand. He spent three years at Pathum Kongka, Bangkok, Thailand for his Junior high school, then attended Trium Udom Sauksa, Bangkok, Thailand for two years for his Senior high school. He passed the external examination at Wat Thart Thong School and achieved a level of Grade 12 in 1988. He obtained his B.S. degree in electrical engineering from Chulalongkorn University in April 1992. After graduation, he worked for Acumen Company on satellite communication systems. His responsibilities mainly dealt with Terrestrial Earth Station by VSAT, both installation and maintenance of the system for customer sites. In 1993, he was awarded a scholarship from the government of Thailand to continue his studies towards Master's and PhD degrees in electrical engineering. His research interests include satellite communications and fiber optics.